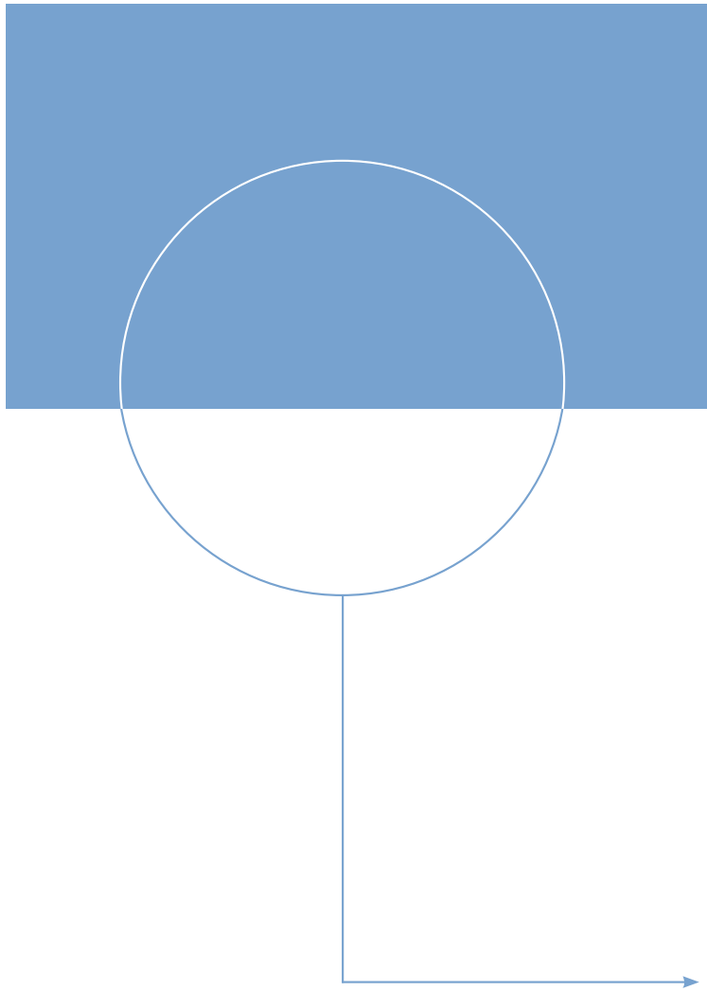

Master's thesis

2019

Ilgar Azizov

NTNU
Norwegian University of
Science and Technology
Faculty of Engineering
Department of Geoscience and Petroleum

Ilgar Azizov

Effect of Water Quality on Wettability Alteration in Carbonates

June 2019

NTNU
Norwegian University of
Science and Technology

NTNU
Norwegian University of
Science and Technology

NTNU
Norwegian University of
Science and Technology

Effect of Water Quality on Wettability Alteration in Carbonates

Ilgar Azizov

Petroleum Engineering
Submission date: June 2019
Supervisor: Carl Fredrik Berg, IGP
Co-supervisor: Ole Torsæter, IGP

Norwegian University of Science and Technology
Department of Geoscience and Petroleum

Summary

The topic of the master's thesis is the wettability alteration in carbonates by Low Salinity enhanced oil recovery (EOR). Wettability alteration towards more water-wet upon reduction of salinity and/or manipulation of ionic composition of brine and consequent additional oil recovery is known as Low Salinity EOR. This master's thesis is the continuation of work done as part of a preliminary study during the master's specialization project. One of the goals of the thesis is to perform wettability alteration study on outcrop carbonate from the Ainsa Basin in the Spanish Pyrenees, which is selected to represent carbonate reservoir rock from a field in Brazil, operated by Equinor. Another goal is to build an experimental base for a wettability alteration study at elevated temperatures on reservoir core samples from the aforementioned field.

The wettability alteration in Ainsa carbonate was studied using the spontaneous imbibition (SI) tests at 96°C. Two sets of experiments, with two core plugs in each for reproducibility of results, were performed. The first set scrutinized influence of salinity reduction on wettability alteration using synthetic formation water (SFW), synthetic seawater (SSW) and ten times diluted SSW (10dSSW) as imbibing brines. While the second set investigated the effect of ionic composition using SSW, SSW with a doubled concentration of sulfate (SSW2SO4) and SSW with a fourfold concentration of sulfate (SSW4SO4).

The SI tests were supported by mineralogy, zeta potential and interfacial tension (IFT) studies. Based on mineralogy study by means of X-Ray Diffraction (XRD) and Energy-dispersive X-ray spectroscopy (EDS), Ainsa carbonate was classified as anhydrite free limestone mainly comprising calcite and quartz. Small amounts of K-feldspar, fluorite, and apatite were found as well. Zeta potential measurements showed that outcrop limestone material is reactive with potential determining ions (PDIs).

The result of SI tests showed that SSW is the most effective EOR fluid for crude oil-brine-rock system used in the experiment. Incremental oil recovery under SSW made up 10-18% of original oil in place (OOIP). When the core plugs were exposed to 10dSSW, after imbibition with SSW, no additional oil recovery was obtained. Imbibition under SSW2SO4 and SSW4SO4 resulted in low additional oil recoveries. SSW2SO4 recovered extra 1.5-3% of OOIP when used as imbibing brine after SSW. SSW4SO4 test on one core plug only extracted an additional 3% after SSW2SO4.

The new experimental setup was build for the SI tests at elevated temperatures on Ainsa carbonate core plugs. This setup allows the change of imbibing brine in the imbibition cell without interruption of the SI test. Overall, the setup performed as expected during the long term SI test and brine replacement. However, a few drawbacks were identified: the valves used for the setup tend to get clogged because of salt precipitation; although the brines were degassed, air bubbles were observed on the surfaces of the core plugs.

Acknowledgements

This thesis is written as part of Master's degree in Petroleum Engineering with specialisation in Reservoir Engineering and Petrophysics at the Norwegian University of Science and Technology (NTNU), Department of Geoscience and Petroleum (IGP).

First of all, I would like to express my profound gratitude to my parents, Irina and Nizami, who emotionally and financially supported me during my studies in Norway. My mother's guidance and continuous support kept me motivated throughout my studies at NTNU.

I would like to thank my supervisor Associate Professor Carl Fredrik Berg for introducing me to the topic, contributing his time to very interesting discussions and sharing his knowledge. I am also grateful to Professor Ole Toræter for sharing his experience and the endorsement of laboratory work at IGP. I would like to express my gratitude to my partner in the laboratory MSc student Marie Bjørdal Løvereide (NTNU), who went with me through numerous issues we had during the experiments, for her support and patience.

My sincere gratitude to Theresia Margaretha Silaen for her love and "stå på" during the challenging times.

Furthermore, I am forever indebted to Ofeliya Ibrahimli who went together with me through two years long journey at NTNU. I am grateful to my friend PhD candidate Salem Akarri (NTNU) for his recommendations regarding laboratory procedures and emotional support. I would like to thank Amine Bouhouche for his life teaching stories, which kept me smiling every day.

I am grateful to Roger Overå (NTNU) and PhD candidate Alberto Luis Bila (NTNU) for sharing their experience and assistance in the laboratory.

Equinor is acknowledged for providing core samples and oil for the experiments.

The Research Council of Norway is acknowledged for the support to the Norwegian Laboratory for Mineral and Materials Characterisation, MiMaC, project number 269842/F50.

Trondheim, 10.06.2019

Table of Contents

List of Tables

List of Figures

Nomenclature

10dFW	=	ten times diluted formation water
10dSSW (10dSW, d10SW)	=	ten times diluted synthetic seawater
100dFW	=	hundred times diluted formation water
25dSW	=	twenty five times diluted synthetic seawater
25dSWEQ	=	25dSW equilibrated with limestone particles
A	=	area
AN	=	acid number
$C_{12}TAB$	=	cationic surfactant trimethyl-ammonium bromide
DI	=	deionized
EDL	=	electric double layer
EDS	=	energy-dispersive x-ray spectroscopy
EOR	=	enhanced oil recovery
HT	=	high temperature
IFT	=	interfacial tension
L	=	oil-limestone contact line
LSE	=	low salinity effect
LSR	=	low salinity recovery
OOIP	=	original oil in place $[cm^3]$
PDI	=	potential determining ion
PTFE	=	polytetrafluoroethylene
SEM	=	scanning electron microscopy
SI	=	spontaneous imbibition
SFW (FW)	=	synthetic formation water
SSW (SW)	=	synthetic seawater
SSW2SO4	=	synthetic seawater with doubled sulfate content
SSW4SO4	=	synthetic seawater with fourfold increased sulfate
TDS	=	total dissolved solids
WI	=	wetting index
WM	=	wettability modifying
XRD	=	x-ray diffraction

A	=	cross-sectional area of the core plug $[cm^2]$
Å	=	angstrom, unit of length $[10^{-10}\ m]$
b	=	Klinkenberg correction factor $[-]$
c_0	=	bulk concentration of a monovalent salt $[\frac{L}{mol}]$
c_i	=	local concentration of i^{th} species of ions $[\frac{number\ of\ ions}{m^3}]$
c_i^0	=	concentration of i^{th} species of ions in the bulk solution $[\frac{number\ of\ ions}{m^3}]$
d	=	average diameter of the core plug $[cm]$
e	=	the electronic charge $[-]$
$f(ka)$	=	Henry's function $[-]$
k_B	=	Boltzmann constant $[-]$
k_g	=	air permeability $[D]$
L	=	average length of the core plug $[cm]$
m	=	slope of the graph $[-]$
P_1	=	upstream pressure $[bar]$
P_2	=	downstream pressure $[bar]$
P_{atm}	=	atmospheric pressure $[atm]$
P_m	=	mean pressure $[atm]$
Q	=	flow rate $[ml/s]$
S_{wir}	=	irreducible water saturation $[-]$
T	=	temperature of the system $[K]$
U_e	=	electrophoretic mobility $[\frac{m^2}{Vs}]$
V_1	=	volume of matrix cup without a core plug $[cm^3]$
V_2	=	volume of matrix cup with a core plug $[cm^3]$
V_{bulk}	=	bulk volume of the core plug $[cm^3]$
V_{grain}	=	total grain volume of the sample $[cm^3]$
V_{pore}	=	pore volume of a core plug $[cm^3]$
V_w	=	volume of produced water $[cm^3]$
W_{dry}	=	weight of the dry core $[g]$
W_{wet}	=	weight of the core saturated with water $[cm^3]$
x, y, z	=	cartesian coordinates
z_i	=	valence of ions $[-]$
ϵ	=	dielectric permittivity $[-]$
ϵ_0	=	vacuum permittivity $[\frac{F}{m}]$
ζ	=	zeta potential $[mV]$
η	=	dynamic viscosity of a liquid $[mPa * s]$
θ	=	contact angle $[-]$
λ_D	=	the Debye length $[m]$
μ	=	air viscosity $[cP]$
ρ_e	=	charge density $[\frac{C}{m^3}]$
ρ_{grain}	=	matrix grain density $[g/cm^3]$
ρ_w	=	density of synthetic formation water $[g/cm^3]$
σ_{os}	=	oil/rock surface interfacial tension $[mN/m]$
σ_{ws}	=	water/rock surface interfacial tension $[mN/m]$
σ_{ow}	=	oil/water interfacial tension $[mN/m]$

ϕ_e = effective porosity $[\%]$
ψ = electric potential $[V]$
ψ_0 = surface potential $[V]$

Chapter 1

Introduction

Generally, carbonate reservoirs are characterized as naturally fractured systems comprising tight very porous matrix blocks and highly permeable fractures. In fractured systems transport of fluids occurs mainly through an interconnected set of fractures, while matrix blocks act as a source of oil. Therefore the effectiveness of water flooding as an EOR method depends on the efficiency of oil displacement from matrix blocks to fractures. The spontaneous imbibition is the primary recovery mechanism of oil recovery from matrix blocks, which is capillary pressure driven (Hirasaki and Zhang, 2004). Effectiveness of oil displacement by the spontaneous imbibition is sensitive to wetting properties of the rock (Morrow, 1990). When wetting property of the matrix is oil-wet, oil is retained by capillarity (Hirasaki and Zhang, 2004). Wettability of carbonate reservoir rock is typically regarded as mixed-wet/preferentially oil-wet (Chilingar and Yen, 1983), which is unfavorable for the imbibition process, making conventional water flooding inefficient. Change of wettability in the matrix towards more water-wet will reduce capillary forces retaining oil and increase the efficiency of oil displacement by the spontaneous imbibition (Hirasaki and Zhang, 2004).

Numerous papers published over the last two decades identified that wettability of carbonate rocks can be changed towards more water-wet conditions by reducing salinity or modifying ionic composition of water (Romanuka et al., 2012; Zhang et al., 2007; Yousef et al., 2011; Mahani et al., 2015; Shariatpanahi et al., 2011; Fathi et al., 2012). In the literature, this EOR technique is commonly referred to as Low Salinity EOR. The incremental oil recovery under Low Salinity EOR has been associated with several mechanisms: electric double layer expansion (Mahani et al., 2017), change of a rock surface charge due to the activity of potential determining ions (PDIs) (Zhang et al., 2006) and dissolution of calcite (Hiorth et al., 2010). Despite the emerging interest towards Low Salinity EOR and research over the past years, it is not possible to predict the response of a specific oil-brine-rock system to Low Salinity EOR and the amount of additional oil recovery (Bartels et al., 2019). Therefore, core analysis experiments are needed to demonstrate the feasibility of

Low Salinity EOR for a particular reservoir.

This master's thesis investigates the effect of Low Salinity EOR on oil recovery from Ainsa carbonate, which is representative of a carbonate field in Brazil operated by Equinor. Preliminary study on outcrop carbonate core plugs from the Ainsa Basin in the Spanish Pyrenees was performed as part of the master's specialization project (Azizov, 2018). Influence of reduced salinity on wettability alteration was studied in the project by spontaneous imbibition tests at 96°C . The experimental setup was assembled for the project to avoid issues related to high temperatures (Pollen and Berg, 2018). However, when the test was interrupted to change the imbibing brine in the imbibition cell it was identified that the assembled setup had certain drawbacks and required further modifications. To clarify, when imbibition cells were emptied, air bubbles started to escape core plugs triggering oil recovery, which compromised the test.

Therefore, **the master's thesis** has two main **objectives**:

1. To build a new experimental setup for spontaneous imbibition tests at elevated temperature (96°C), which provides the capability of imbibing brine replacement without interruption of the test;

2. To use the new experimental setup to scrutinize influence of salinity and ion composition of imbibing brine on enhanced oil recovery from the outcrop Ainsa carbonate.

Based on the aforementioned preliminary study it is expected to obtain additional oil recovery from Ainsa outcrop carbonate upon reduction of salinity of imbibing brine. It is reported in literature that outcrop carbonate material can be unresponsive to the activity of potential determining ions and yield misleading results (Ravari, 2011). On the other hand, it is believed that anhydrite present in rock matrix (source of PDIs) can result in significant incremental oil recovery (Austad et al., 2015). A comprehensive study of mineralogy and reactivity of Ainsa carbonate to PDIs is performed to support the set of experiments scrutinizing the influence of ion composition on wettability alteration. It is expected to use newly built experimental setup and obtained data to perform spontaneous imbibition tests on reservoir rock material from carbonate field in Brazil as part of a future study.

The **structure of the master's thesis** is as follows:

- Chapter 1: Presents the topic of the study, provides information about the preliminary study, states the objectives and describes the structure of the thesis.

- Chapter 2: Discusses the factors influencing initial wetting in carbonates. Secondly, investigates the experiments published in literature to build background about the mechanisms underlying Low Salinity EOR. Additionally, provides an overview of experimental approaches followed for Low Salinity EOR studies. This chapter is reworked and expanded version of the Background chapter in master's specialization project (Azizov, 2018).

- Chapter 3: Gives information about the Electric Double Layer Theory, which describes behaviour of ions in the vicinity of charged surfaces. This chapter is similar to the Theory chapter in master's specialization project (Azizov, 2018).

- Chapter 4: Describes the new experimental setup and protocols followed. Secondly, provides information about methods and materials used for wettablity study on outcrop core plugs from the Ainsa Basin the in Spanish Pyrenees.
- Chapter 5: Presents all the results of the study and discusses them. Moreover discusses behaviour of the new experimental setup and issues arose during the long term spontaneous imbibition tests.
- Chapter 6: The conclusions of Low Salinity EOR study on outcrop core plug from Ainsa selected to represent reservoir rock are presented. Finally, recommendations are given on how to improve the experimental setup and gain a better understanding of the effect of Low Salinity EOR on reservoir rock material from the field in Brazil in a future study.

Chapter 2

Background

This chapter firstly discusses parameters influencing wetting in carbonates. Secondly, experiments published in the literature are presented, and proposed mechanisms underlying wettability alteration in carbonates are discussed. The dissolution of calcite is not considered in this chapter as this mechanism will not contribute at a reservoir scale (Mahani et al., 2017). Last but not least, experimental approaches applied in the wettability alteration studies are presented. The content in this chapter is connected to the Electric Double Layer Theory presented in chapter 3.

2.1 Initial Wetting of Carbonates

The electrical potential of the oil-brine interface and rock-brine interface is one of the most important parameters dictating the wetting property of the rock surface (Hirasaki, 1991). Measurements of zeta potential showed that surface charge at the oil-brine interface is negatively charged (Mahani et al., 2015), while calcite-brine interface is believed to have positive charge for pH<9.5 and formation water with high content of Ca^{2+} (Zhang and Austad, 2005). Van der Waals and electrostatic forces promotes attraction between two oppositely charged interfaces. This causes instability of the water film between oil and the rock leading to adsorption of carboxylic groups from oil onto the carbonate rock surface (Legens et al., 1999). Carboxylic acids bind very strongly to carbonate surface at near neutral pH $<$ 8-9, and this bonds are nearly irreversible (Thomas et al., 1993).

The amount of carboxylic material in crude oil is determined by the acid number (AN) (mg KOH/g) (Zhang and Austad, 2005). The Figure 2.1 depicts effect of various AN of the crude oil on spontaneous imbibition of water into chalk cores. The higher is the AN of the crude oil, the lower is the imbibition rate and recovery (Standnes and Austad, 2000). Similar results were observed by Zhang and Austad (2005) in a series of experiments on chalk core plugs. They concluded that AN of crude oil influences the extent of the water

wetness of the carbonate rock. As the AN of the crude oil increases, the water wetness of the rock decreases.

Sulfate is known to be a potential determining ion (see subsection 3.1.3) to carbonate rock surface (Strand et al., 2006b). Presence of sulfate in formation water has significant effect on initial wetting of carbonates (Shariatpanahi et al., 2011). Figure 2.2 illustrates wetting index of cores containing 0 and 0.002 mol/l of sulfate in the formation water at different aging temperatures. Even insignificant amount of sulfate dramatically changes wettability of the rock towards more water-wet. Adsorption of carboxylic material is hindered by sulfate ions available in formation water making wetting conditions of the rock surface to be more water-wet (Shariatpanahi et al., 2011). Mechanism behind this phenomenon is discussed in subsection 2.2.1.1.

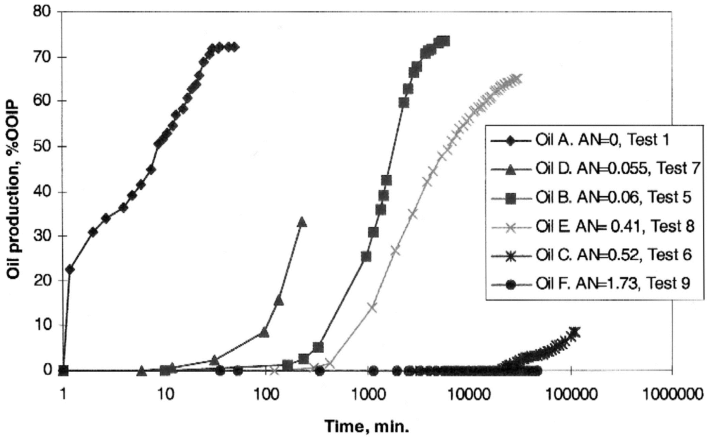

Figure 2.1: Spontaneous imbibition into chalk cores saturated with oils having different acid number. Figure from Standnes and Austad (2000).

A study by Mjos et al. (2018) showed that an increase in the surface area of the rock available for polar components, e.g. carboxylic material, decreases water wetness of the rock. Therefore, reducing initial water saturation of the core plugs makes the rock surface less water-wet.

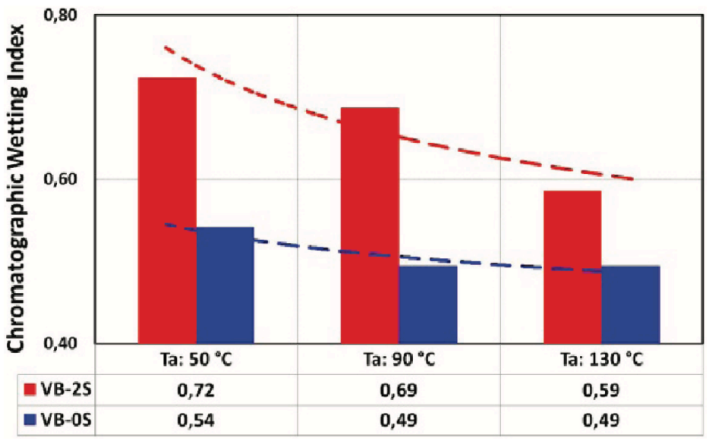

Figure 2.2: Wetting index (WI) of the cores containing 0 and 0.002 mol/l of sulfate in formation water at different aging temperatures. WI describes water-wet fraction of rock surface. Figure from Shariatpanahi et al. (2011).

2.2 Wettability Alteration in Carbonates

2.2.1 Influence of Ionic Composition

Strand et al. (2003) investigated how cationic surfactant, $C_{12}TAB$, in presence of sulfate added to the brine affect the imbibition process and wettability alteration in chalk and dolomite core plugs. They discovered that increase in concentration of sulfate and elevated temperature improves the performance of spontaneous imbibition. Moreover, chalk cores were more sensitive to sulfate concentration than dolomite, which was confirmed by contact angle measurements as well. This triggered further studies to scrutinize the influence of PDIs (Ca^{2+}, Mg^{2+} and SO_4^{2-}) and temperature on wettability alteration of carbonates, and explain mechanism underlying change of wetting properties of the carbonates.

2.2.1.1 Chalk

Effect of SO_4^{2-}. Zhang and Austad (2006) scrutinized influence of sulfate on wettablity alteration in a number of spontaneous imbibition tests conducted on an outcrop chalk from Stevns Klint at 70, 100 and 130°C. The concentration of SO_4^{2-} in the imbibing fluid was varied to 4, 2, 1/4 and 0 times of that present in SW, while the content of Ca^{2+} was kept constant to avoid its effect on imbibition process (Strand et al., 2006b). Ionic strength of the imbibing fluids remained unchanged by tuning concentration of NaCl. The results of experiments conducted at 70°C are depicted in Figure 2.3. The oil recovery increased significantly from about 15% to 55% at 70°C as the concentration of sulfate increased.

Figure 2.4 depicts zeta potential measurements of a chalk particles in suspension performed by Zhang and Austad (2006). The measurements demonstrate that zeta potential tends to more negative values with increase in concentration of SO_4^{2-}, indicating an affinity of the anion to the chalk surface. Adsorption of SO_4^{2-} to positively charged water-wet sites cause stronger electrostatic repulsion between the chalk surface and negatively charged carboxylic material, $R - COOH^-$. This releases carboxylic material from chalk surface and makes it more water-wet. Therefore, Zhang and Austad (2006) associated increase in oil recovery with wettability alteration due to adsorption of SO_4^{2-} to positive chalk surface. It is essential to highlight that diminishing amount of NaCl in imbibing fluid leads to increase in water-wet fraction of carbonate rock (see Figure 2.5) and the impact is more remarkable at higher temperatures (Fathi et al., 2012). Since amount of NaCl in imbibing fluids was modified, one might argue that influence of SO_4^{2-} on wettability alteration was intensified by lower NaCl concentration.

The effect of temperature on oil recovery related to different sulfate concentration in the imbibing fluid is illustrated in Figure 2.6 (Zhang and Austad, 2006). At 130°C an increase in the concentration of sulfate beyond the level present in seawater did not result in significant oil recovery growth. On the other hand, fourfold increase in sulfate concentration at 100°C almost doubled the oil recovery. Overall, it is seen that at 130°C the oil recovery was significantly higher than that at 100°C for all imbibing fluids .

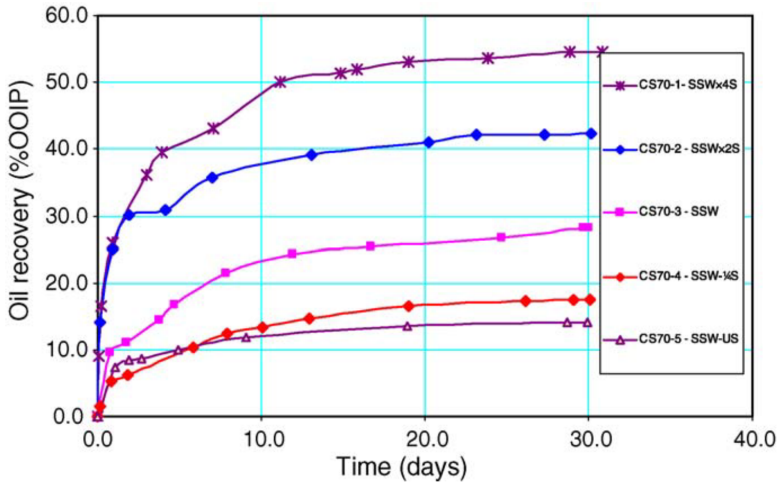

Figure 2.3: Spontaneous imbibition test at 70°C using imbibing fluids with different SO_4^{2-} concentrations. Figure from Zhang and Austad (2006).

Strand et al. (2006b) examined SO_4^{2-} adsorption onto the Stevns Klint chalk surface at 23, 70, 100 and 130°C using a new wettability estimation technique (Strand et al., 2006a). The method is based on chromatographic separation of the non-adsorbing tracer, SCN^-, and SO_4^{2-} at water wet sites while flooding a porous system. The effluent concentrations of the tracer and SO_4^{2-} are plotted versus pore volume injected. The larger the area (A)

between the effluent curves for the two components, the higher the fraction of the water-wet area in a core sample. The fraction of the water-wet area represents the new wetting index. Figure 2.7 shows the results of chromatographic separation test. It is seen that the area between effluent curves increases as temperature rises. This indicates that affinity of SO_4^{2-} to the chalk surface is temperature dependant and intensifies as temperature increases.

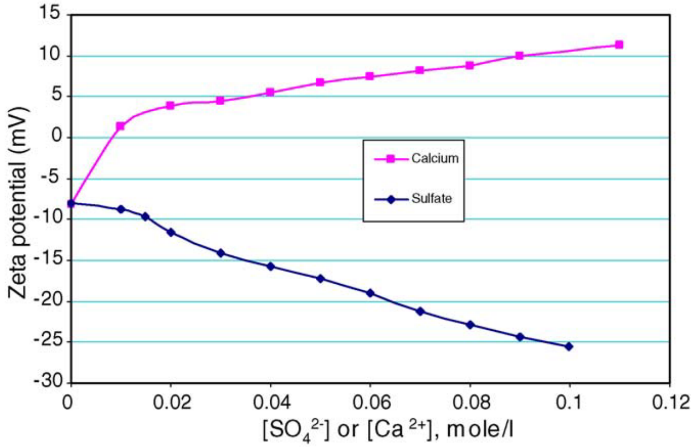

Figure 2.4: Zeta potential measurement on aqueous chalk suspension at pH 8.4. Figure from Zhang and Austad (2006).

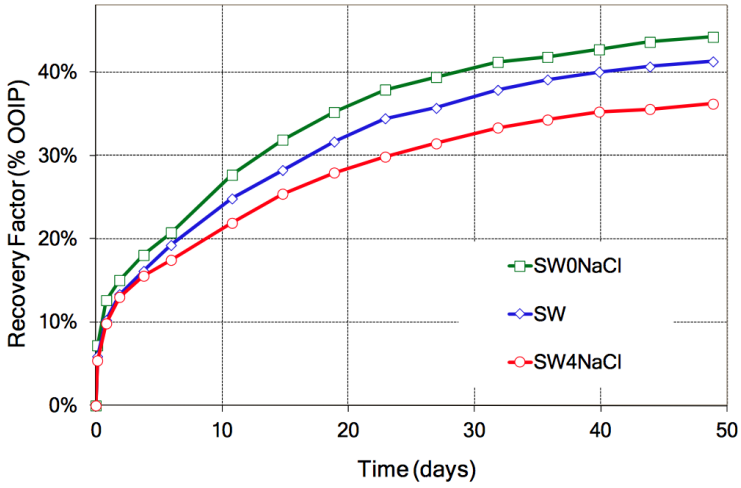

Figure 2.5: Diminishing of NaCl content in imbibing brine increases oil recovery. Figure from Fathi et al. (2012).

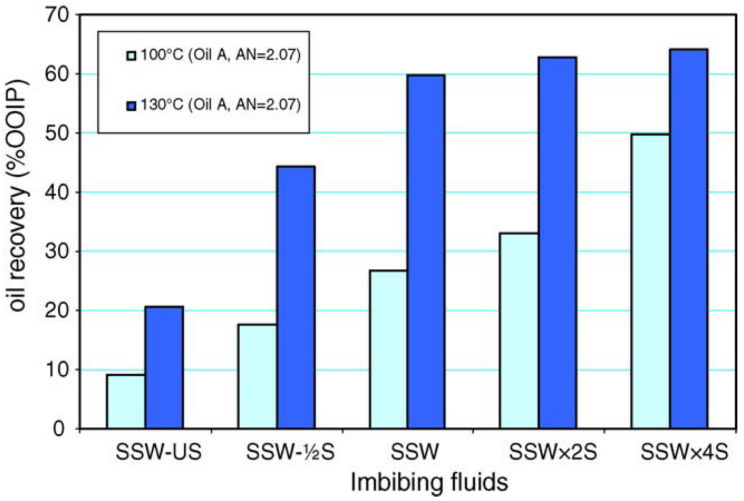

Figure 2.6: Comparison of maximum oil recovery at 100°C and 130°C when imbibing waters with various sulfate content were used. Figure from Zhang and Austad (2006).

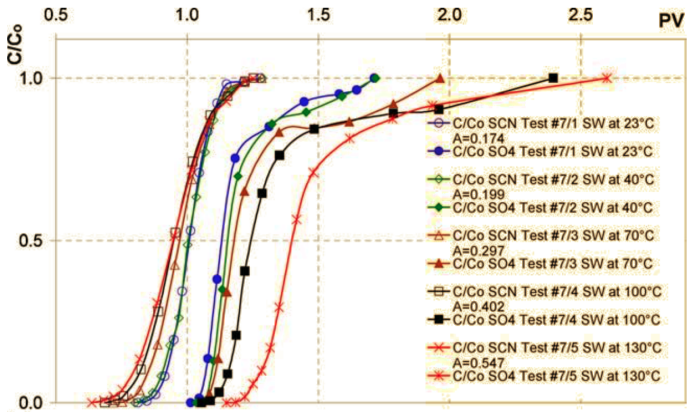

Figure 2.7: Affinity of SO_4^{2-} to the chalk surface at various temperatures using chromatographic separation technique. Concentrations of SO_4^{2-} and Ca^{2+} are equal to those in seawater. Area (A) increases as temperature rises. Figure from Strand et al. (2006b).

Effect of Ca^{2+}. Zhang and Austad (2006) demonstrated that zeta potential changes upon addition of Ca^{2+} into an aqueous chalk suspension (see Figure 2.4) indicating that Ca^{2+} is a PDI to chalk surfaces. Strand et al. (2006b) investigated affinity of sulfate to chalk surface at different Ca^{2+} concentrations and various temperatures by coreflooding using chromatographic separation technique (Strand et al., 2006a). The concentration of Ca^{2+} was varied to 3, 2, 1, 1/2 and 1/4 times of its concentration in seawater, while the total dissolved solids (TDS) were kept constant by tuning the amount of NaCl. The SO_4^{2-} content in all brines used for chromatographic tests was constant and equal to the one present in

seawater. The results of the experiments conducted at 100 and 130°C are shown in Figure 2.8. It is seen that the area between the effluent curves increases as the temperature and concentration of Ca^{2+} rises suggesting that affinity of SO_4^{2-} to chalk intensifies.

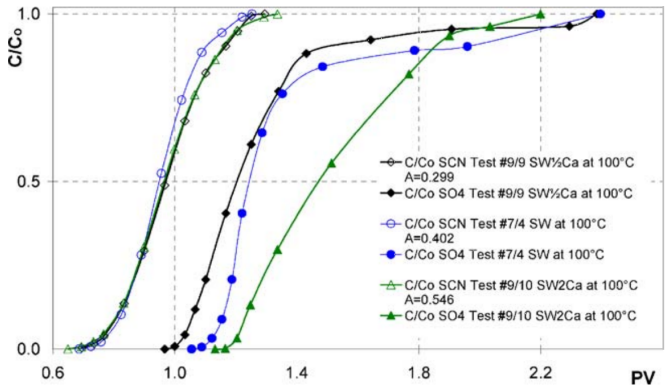

(a) Sulfate adsorption at 100°C.

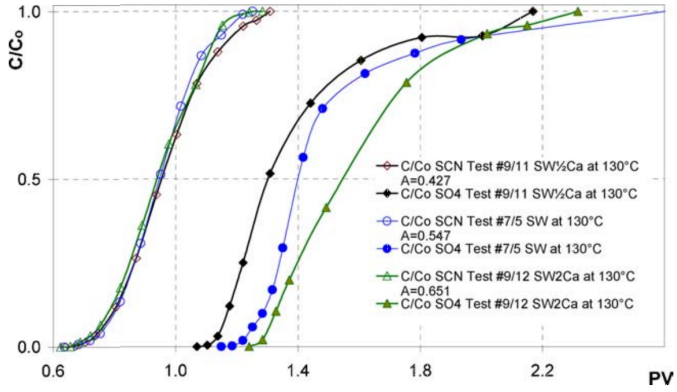

(b) Sulfate adsorption at 130°C.

Figure 2.8: Chromatographic separation tests at 100°C and 130°C. Ca^{2+} is varying 1/2 and 2 times of the concentration in seawater. Sulfate concentration is constant and equal to that in seawater. Area (A) increases as temperature rises. Figure from (Strand et al., 2006b).

It is determined by Strand et al. (2006b) that adsorption of sulfate to the rock surface increases with temperature (see Figure 2.7). Strand et al. (2006b) studied adsorption of Ca^{2+} towards chalk surface at different temperatures by coreflooding. Figure 2.9 shows that the concentration of Ca^{2+} in the effluent decreases as the core plug is flooded until adsorption equilibrium is established and Ca^{2+} returns to initial concentration. It is also observed that adsorption of Ca^{2+} towards chalk surface increases during flooding with increasing temperature as well.

From their observation Strand et al. (2006b) suggested that interplay between SO_4^{2-} and

Ca^{2+} play an important role in wettability alteration in carbonates. They propose that adsorption of sulfate to positive rock surface creates less electrostatic repulsion with co-ions, which attracts Ca^{2+} to the surface. Attracted to the surface Ca^{2+} creates a complex with organic carboxylic material removing it from the rock surface and promoting sulfate attachment to available surface site.

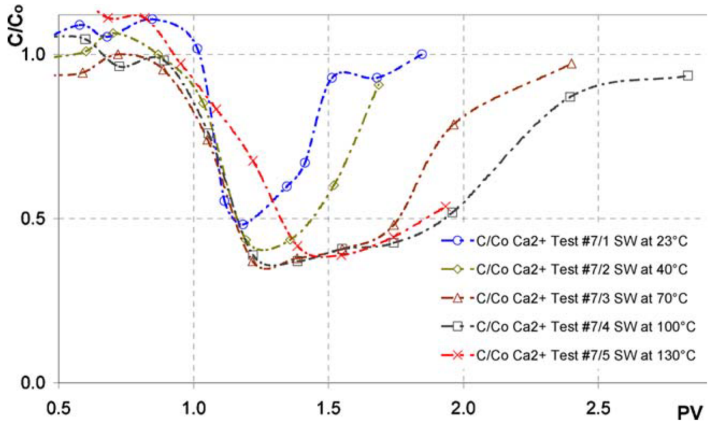

Figure 2.9: Concentration of Ca^{2+} in effluent after flooding chalk core plug at various temperatures. Figure from Strand et al. (2006b).

Effect of Mg^{2+}. Zhang et al. (2007) studied the impact of Mg^{2+} on the wettability alteration process. They were motivated by the following facts:

- Mg^{2+} makes up the largest concentration of divalent ions in seawater
- At elevated temperatures, Ca^{2+} is replaced in the surface lattice of biogenic outcrop chalk by Mg^{2+} (Korsnes et al., 2006).
- Decrease in the content of Mg^{2+} was registered after breakthrough of injected seawater in the chalk Ekofisk field (reservoir temperature is 130°C) (Petrovich and Hamouda, 1998).

Zeta potential measurements executed on aqueous chalk suspension as part of the study showed that Mg^{2+} is PDI to chalk surface. The chromatographic separation technique was used to compare the ability of Mg^{2+} and Ca^{2+} to adsorb on chalk surface. Sodium chloride solution containing equal amount of Mg^{2+} and Ca^{2+} was flooded through the chalk core. Results illustrated in Figure 2.10a shows that the area between the effluent curve of tracer, SCN^-, and Ca^{2+} is larger than that for SCN^- and Mg^{2+}. This indicates weaker affinity of Mg^{2+} than Ca^{2+} to chalk surface at 23°C.

Similar chromatographic test executed at 130° showed increase in adsorption of Mg^{2+} to chalk (see Figure 2.10b). Moreover, amount of Ca^{2+} in effluent significantly exceeded initial concentration, which was explained by replacement of Ca^{2+} with Mg^{2+} in the rock lattice. Therefore, it was concluded that activity of Mg^{2+} intensifies at high temperatures.

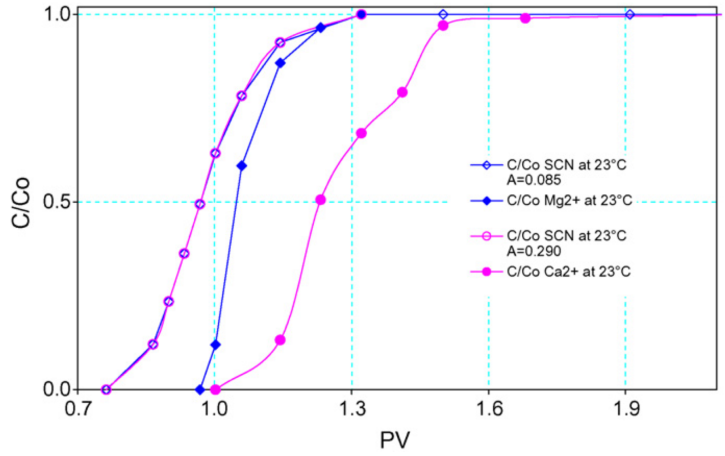

(a) Competitive adsorption of Ca^{2+} and Mg^{2+} at 23°C

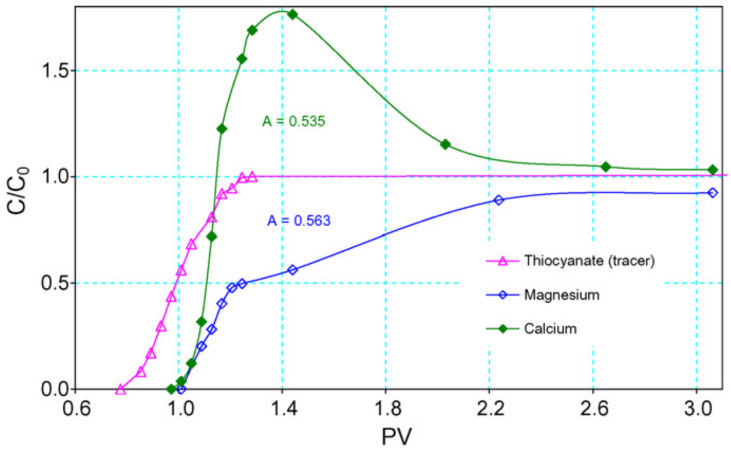

(b) Competitive adsorption of Ca^{2+} and Mg^{2+} at 130°C

Figure 2.10: Affinity of Mg^{2+} towards oil-wet chalk surface at 23°C and 130°C. Figure from Zhang et al. (2007).

Results of spontaneous imbibition tests performed by Zhang et al. (2007) on four chalk cores saturated with NaCl solution as initial brine are depicted in Figure 2.11. The aim of the tests was to investigate the effect of PDIs and temperature combined on oil recovery.

First, the cores were left for imbibition at 70°C in a NaCl solution free of Ca^{2+} and Mg^{2+} and containing 0, 1, 2 and 4 times the concentration of sulfate present in seawater. Oil recovery from all the cores was approximately 10%, which was related to escape of oil from the cores because of fluid expansion. When temperature was elevated to 100°C, slight increase in recovery was observed because of additional expansion of the fluids. At this point it was determined that SO_4^{2-} cannot improve oil recovery from the chalk

core in the absence of other PDIs. The oil production soared at 100°C when either Ca^{2+} or Mg^{2+} (in the concentrations present in seawater) were added into the imbibing water. When temperature was increased to 130 °C, imbibing water containing Ca^{2+} and twice the concentration of SO_4^{2-} present in seawater showed similar effect on oil recovery as imbibing water containing Mg^{2+} and 0 times SO_4^{2-} compared to sea water. The oil recovery increased in both tests , however this recovery increment was assummed to be related to fluid expansion. This observation showed that activity of Ca^{2+} is hindered at high temperatures because of $CaSO_4$ precipitation. For the rest of imbibing waters which was spiked with Mg^{2+}, the oil recovery was related to SO_4^{2-} concentration. Imbibing waters containing 1 and 2 times SO_4^{2-} concentration present in seawater led to the oil recovery about 50% and 60% respectively.

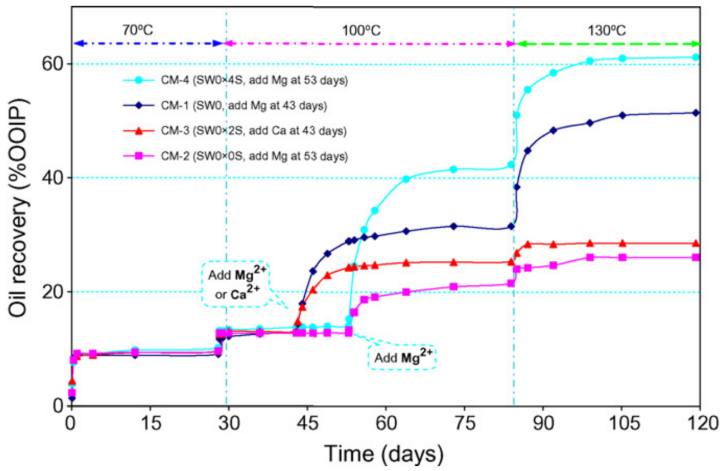

Figure 2.11: The effect of PDIs on spontaneous imbibition into chalk core at 70, 100 and 130°C. Ca^{2+} and Mg^{2+} were added to imbibing water either at 43^{rd} or 53^{rd} day of the experiment. Figure from Zhang et al. (2007).

Suggested Mechanism

Based on the above mentioned studies wettability alteration mechanism at low and high temperatures is summarized in Figure 2.12a and Figure 2.12b respectively (Zhang et al., 2007). Initially, sulfate is attracted to the rock surface because of having opposite charge and adsorbs onto it. This changes the surface charge to less positively charged which draws Ca^{2+} close to the rock surface. At low temperatures Ca^{2+} reacts with carboxylic groups displacing them from the rock surface by the following reaction:

$$\begin{aligned} &RCOO^- - Ca - CaCo_3(s) + Ca^{2+} + SO_4^{2-} = \\ &= RCOO^- - Ca^{2+} + Ca - CaCo_3(s) + SO_4^{2-} \end{aligned} \tag{2.1}$$

At high temperatures Mg^{2+} becomes more active and is able to displace Ca^{2+} from the rock lattice together with the carboxylic material connected to it according to the following

reaction:

$$RCOO^- - Ca - CaCo_3(s) + Mg^{2+} + SO_4^{2-} = \\ = RCOO^- - Ca^{2+} + Mg - CaCo_3(s) + SO_4^{2-} \tag{2.2}$$

The effect of the suggested wettability alteration mechanism can be summarised as follows:

- SO_4^{2-} acts as a catalyst stimulating an increase in the concentration of Mg^{2+} and Ca^{2+} close to the rock surface;
- SO_4^{2-} is not able to alter wettability in the absence of Mg^{2+} and Ca^{2+} ;
- The wettability alteration process is effective at temperatures higher than 90°C.

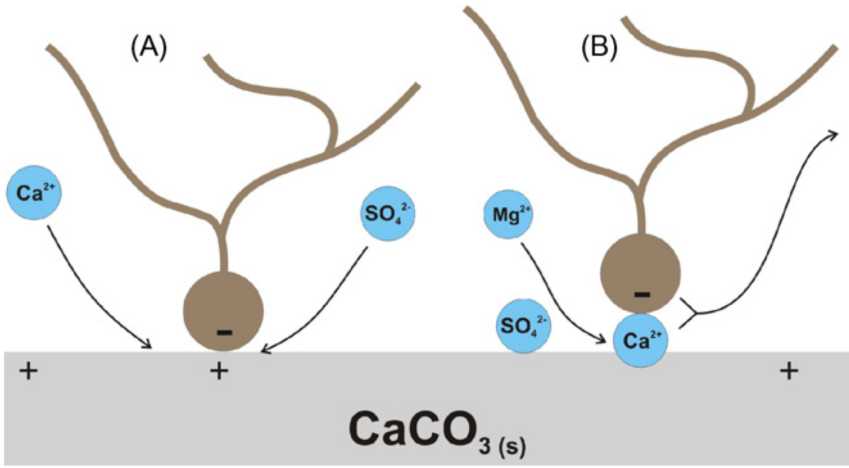

Figure 2.12: Schematic of wettability alteration mechanism proposed by Zhang et al. (2007): a) the mechanism at low temperatures, b) the mechanism at high temperatures. Figure from Zhang et al. (2007).

2.2.1.2 Limestone

Several studies suggests that chalk, because of its biogenic origin, is a lot more responsive to wettability alteration in comparison with limestone (Strand et al., 2008; Mahani et al., 2017). Chromatographic separation tests and spontaneous imbibition experiments were performed by Strand et al. (2008) to investigate if the wettability alteration mechanism proposed for chalk is also relevant for limestone. Reservoir limestone core plugs were flooded with sodium chloride solution containing equal amount of Mg^{2+} and Ca^{2+} to investigate symbiotic interaction between divalent cations in the wettability alteration process. Figure 2.13 shows that at high temperatures there is no increase of Ca^{2+} in the effluent compared to chromatographic separation tests on chalk core (see Figure 2.10b). Hence, it was concluded that Mg^{2+} is less reactive with limestone surface than with chalk.

Similar to the experiments performed on chalk cores, the area between the tracer curve and Mg^{2+} curve is larger than that for tracer and Ca^{2+} curves, which indicates that at high temperatures Mg^{2+} is a more active PDI. On the other hand, when similar test was performed in the presence of SO_4^{2-} (using SW) it was observed that concentration of Ca^{2+} increases in the effluent comparable to the experiment with chalk.

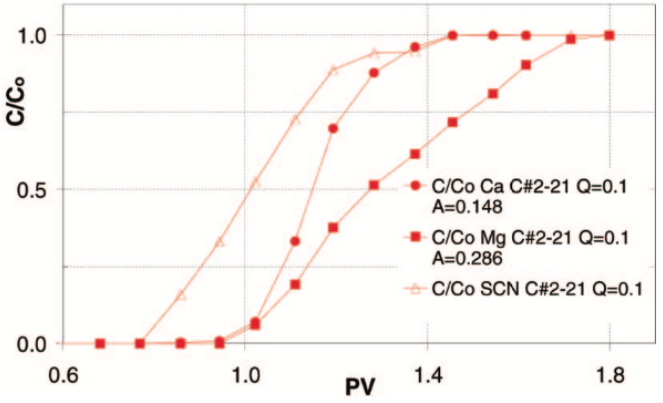

Figure 2.13: Effluent curves. Competitive adsorption test of Ca^{2+} and Mg^{2+} at 130°C. Figure from Strand et al. (2008).

Furthermore, Strand et al. (2008) examined affinity of SO_4^{2-} to the limestone surface using chromatographic separation test. Results showed that SO_4^{2-} is able to adsorb on limestone rock surface similar to the adsorption onto the chalk. Mahani et al. (2017) also demonstrated that SO_4^{2-} is a PDI to limestone by zeta-potential measurements. Figure 2.14 shows that increasing sulfate concentration in aqueous limestone suspension leads to a more negative zeta-potential.

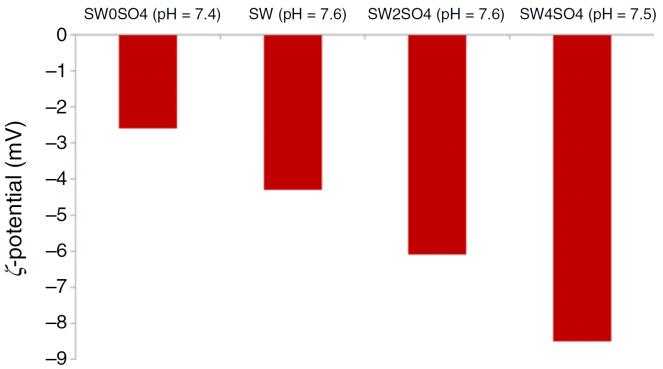

Figure 2.14: Zeta-potential measurements on aqueous limestone suspension with SO_4^{2-} concentration 4, 2 and 0 times of that present in seawater. Figure from Mahani et al. (2017).

Spontaneous imbibition tests performed by Strand et al. (2008) showed that SO_4^{2-} is a catalyst in the wettability alteration process in limestone. The experiment was conducted at 120°C. One core plug was left to spontaneously imbibe in seawater with SO_4^{2-} (SW), while another core in seawater without SO_4^{2-} (SW0S). Sodium chloride was added to SW0S to equalize its salinity to the one present in SW. Figure 2.15 shows that the oil recovery from the cores exposed to SW and SW0S was about 30% and 15% respectively. The oil recovery from the core exposed to SW0S was related to thermal expansion and inhomogeneities in wetting state.

Tests performed on chalk cores showed that seawater spiked with SO_4^{2-} had a positive impact on the oil recovery (Zhang and Austad, 2006). However, increase in the concentration of SO_4^{2-} in SW did not lead to increase in the oil recovery for limestone cores which was associated with $CaSO_4$ precipitation because of high sulfate concentration. It is worth to note that the oil recovery for both cores reached approximately 60% when 1 wt% of the cationic surfactant trimethyl-ammonium bromide, $C_{12}TAB$, was added to imbibing water. This suggests that difference in rock properties is eliminated as the reason for different oil recovery by spontaneous imbibition with SW and SW0S (Strand et al., 2008). From their experiments Strand et al. (2008) concluded that interactions between PDIs and limestone are similar to those observed for chalk.

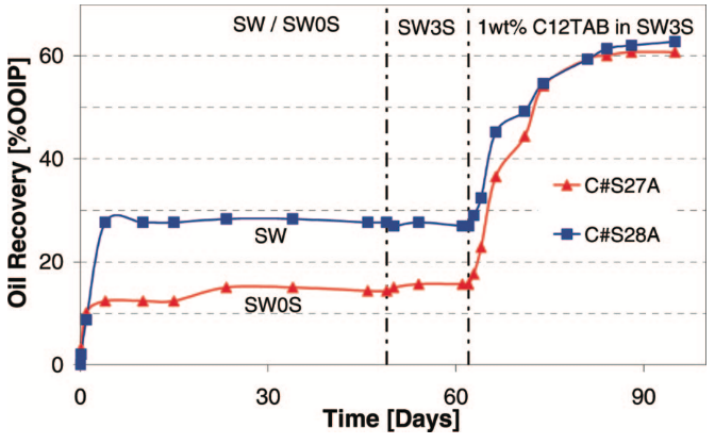

Figure 2.15: Spontaneous imbibition into reservoir limestone core plug at 120°C using SW and SW0S as imbibing fluids. Figure from Strand et al. (2008).

On the other hand, Ravari (2011) demonstrated that reactivity of PDIs with an outcrop limestone is different from a reservoir limestone. The chromatographic separation tests and zeta potential measurements was performed on an outcrop limestone samples obtained from two different locations. The results suggest that affinity of sulfate to the outcrop limestone is very weak and surface charge cannot be decreased to the same extent as for a chalk or reservoir limestone. The spontaneous imbibition tests combined with forced imbibition tests showed that SW is not capable to improve oil recovery from the outcrop limestone samples. Ravari (2011) concluded outcrop limestone can act as non reactive

towards PDIs and lead to misleading results when selected to represent reservoir rock for wettability alteration studies.

2.2.2 Influence of Brine Salinity

It is discussed in subsection 2.2.1 that PDIs play a vital role in wettability alteration mechanism in carbonates. Although dilution of seawater leads to decrease in the overall concentration of PDIs, numerous studies showed that there is a potential to improve oil recovery (Yousef et al., 2011; Nasralla et al., 2018; Romanuka et al., 2012; Shariatpanahi et al., 2016).

Yousef et al. (2011) used several methods to investigate influence of low salinity on wettability alteration in carbonates at reservoir conditions. The X-ray Diffraction (XRD) technique used to find composition of a rock material, used for the studies, showed following mineralogy: 80% calcite, 13% dolomite, 6% anhydrite and less than 1% quartz. Figure 2.16 depicts three sets of contact angle measurements performed by Yousef et al. (2011). The results show that contact angle decreases as the oil droplet is sequentially introduced to less saline water. This indicates that seawater and diluted versions of seawater have a substantial potential to alter wettablity of the carbonate rock to more water-wet. The contact angle method as a quantitative wettability measurement is reviewed elsewhere (Anderson, 1986).

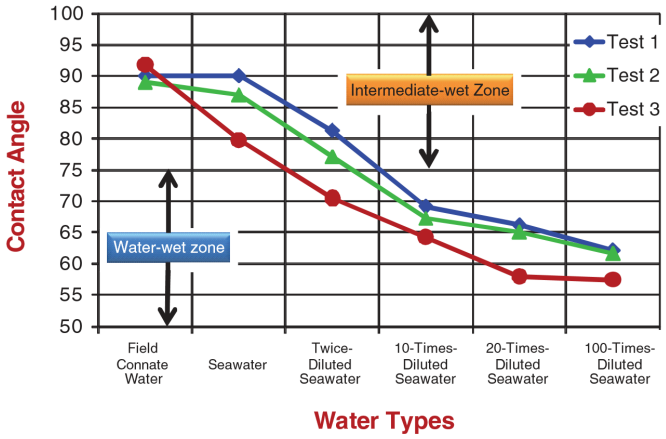

Figure 2.16: Contact angle measurements of crude the oil drops deposited on carbonate rock sample at different water salinities. Figure from Yousef et al. (2011).

Yousef et al. (2011) executed coreflooding experiments on two composite carbonate core plugs using brines of various salinity. The result of only one of the tests is depicted in Figure 2.17, however both core plugs showed comparable response to injection brines. Initially, the core plugs were flooded with seawater until no more oil was produced. After sequentially switching to twice diluted and 10 times diluted seawater notable incremental

oil recovery was achieved. On the other hand, there was no incremental oil recovery when the core plugs were flooded with 20 time diluted and 100 times dilutes seawater.

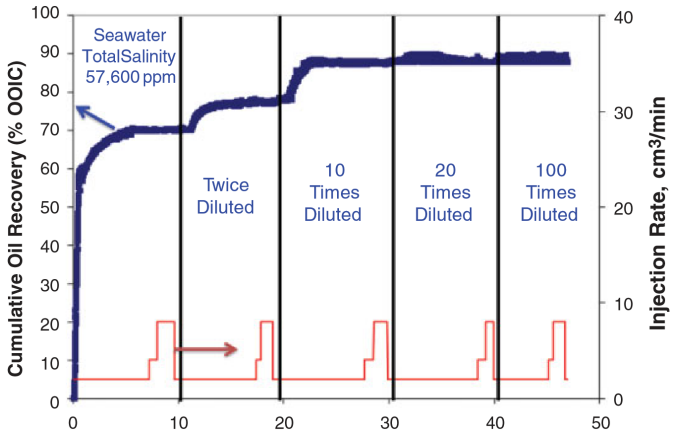

Figure 2.17: Result of composite catbonate core flooding with injection brines of various salinities. Figure from Yousef et al. (2011).

The results of interfacial tension (IFT) measurements on the brines used by Yousef et al. (2011) for coreflooding and contact angle experiments are displayed in Figure 2.18. It is seen that switch from formation water to seawater caused notable IFT reduction by approximately 6 units. Starting from seawater down to 100 times diluted seawater, IFT reduction by 1-2 units for every step was observed. This suggests that dilution of seawater had minor effect on IFT and fluid/fluid interaction during the coreflooding experiments (Yousef et al., 2011). Influence of salinity on IFT was also studied by Al-Khafaji and Wen (2019). They showed similar trends for oils with varying compositions: IFT reduction by 3-5 units when formation water was replaced with seawater and small IFT change for diluted versions of seawater.

Austad et al. (2012) reported incremental oil recovery when flooding limestone core, from the aqueous zone of reservoir, sequentially with formation water (FW) and 100 times diluted formation water (100dFW). Figure 2.19 shows that the oil recovery increased by 5% when salinity of injection brine was reduced. Although FW and 100dFW did not contain any SO_4^{2-}, presence of the PDI was recorded in the effluent. Dissolution of anhydrite present in the rock matrix was proposed as the source of SO_4^{2-} (Austad et al., 2012).

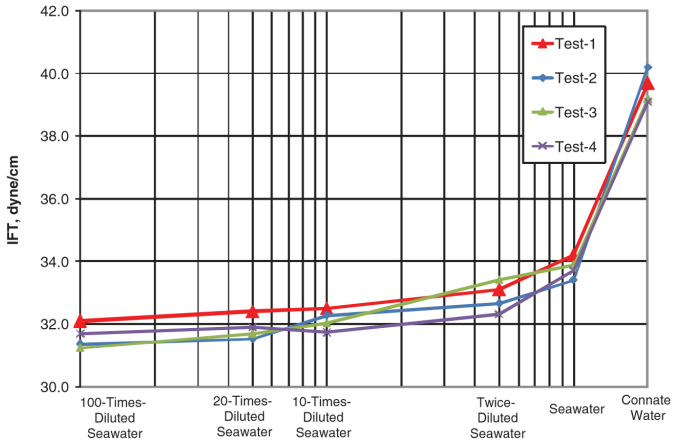

Figure 2.18: IFT measurements of live oil with various brines at reservoir conditions. Figure from Yousef et al. (2011).

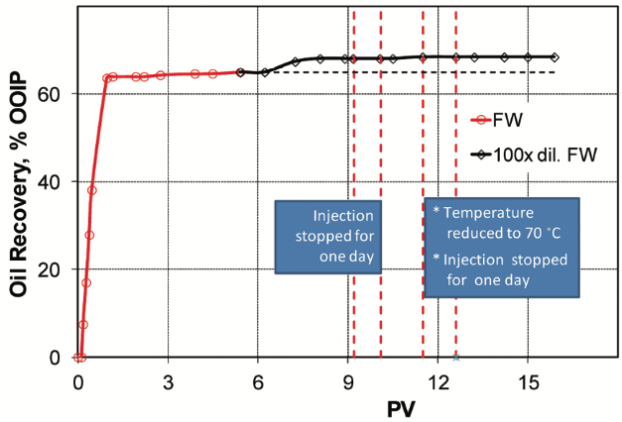

Figure 2.19: The oil recovery from limestone core by using formation water at 110°C and 100dFW at 70°C as injection brines. Figure from Austad et al. (2012).

To validate that increase in the oil recovery is related to anhydrite dissolution and consequent SO_4^{2-} availability, Austad et al. (2012) performed a test on anhydrite free outcrop chalk. Figure 2.20 shows that in the secondary mode the oil recovery was approximately 57%, but no extra oil was recovered from the chalk core after switching to 100dFW. Austad et al. (2012) concluded that additional oil recovery can be obtained by reduced salinity brine when anhydrite is present in the matrix of carbonate rock. Austad et al. (2015) also report anhydrite dissolution and increased oil recovery when limestone reservoir core plug was flooded with FW and 100dFW successively. Moreover, they showed that diluted version of seawater significantly increase oil recovery from limestone core plugs containing

anhydrite. The incremental oil recovery made up 5% and 18% for 10 times diluted and 30 times diluted seawater respectively.

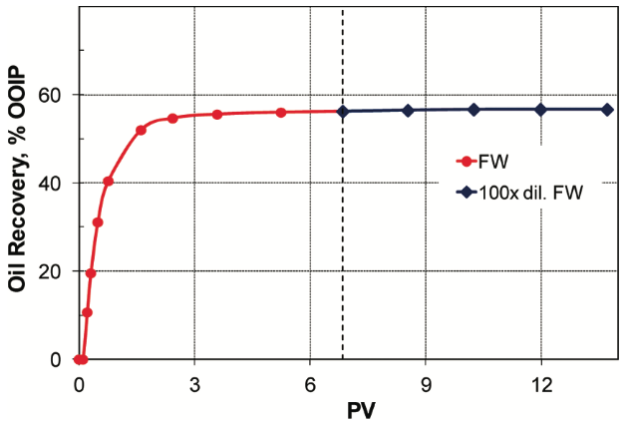

Figure 2.20: Oil recovery from chalk core by using formation water and 100dFW at at 110°C as injection brines. Figure from Austad et al. (2012).

On the other hand, Shariatpanahi et al. (2016) achieved increased oil recovery by low salinity flooding from Silurian outcrop dolomite cores, which did not contain anhydrite. Spontaneous imbibition test performed on two Silurian outcrop dolomite cores at 70°C are depicted in Figure 2.21. Both cores responded similarly to different imbibing fluids. The results show that seawater is not as effective low salinity fluid for dolomite as d10SW. The oil recovery did not increase significantly when the imbibing fluid was changed from formation water to SW, but soared after switching to d10SW. Shariatpanahi et al. (2016) emphasize that role of SO_4^{2-} is still vital since 10dFW free of SO_4^{2-} did not increase oil recovery when followed FW in a similar spontaneous imbibition test on dolomite core. In line with Shariatpanahi et al. (2016) other authors report incremental oil recovery from anhydrite free limestone core plugs using seawater and diluted seawater sequentially in spontaneous imbibition tests (Romanuka et al., 2012; Nasralla et al., 2018).

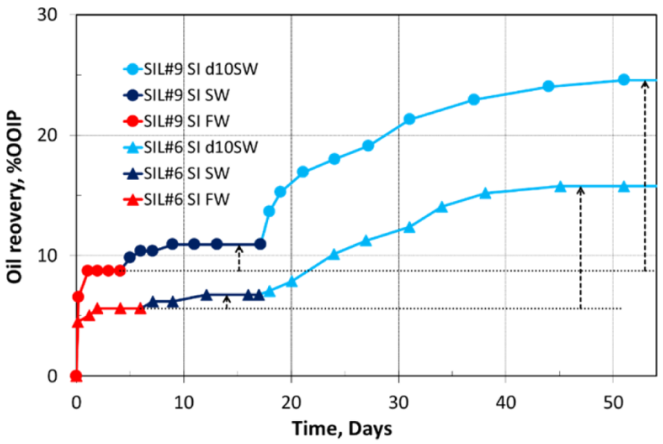

Figure 2.21: The oil recovery from dolomite cores by using formation water, SW and d10SW at 70°C as imbibing fluids. Figure from Shariatpanahi et al. (2016).

Mahani et al. (2017) describe wettability alteration mechanism in terms of electrokinetics of carbonate-brine interface. According to them two main factors causing wettability alteration in carbonates are expansion of electric double layer (EDL) triggered by reduced salinity and adsorption of PDIs to the rock surface forming charged surface complexes. Therefore wettability alteration mechanism is a function of salinity and composition of water as shown in Figure 2.22. First EDL expands (see subsection 3.1.2) and then surface reactions and surface charge change takes place (see subsection 2.2.1). This causes more negative zeta-potential and allows repulsion between rock surface and negatively charged oil-brine interface.

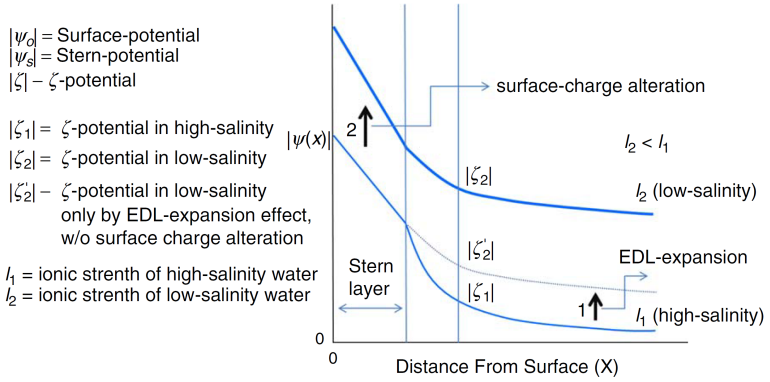

Figure 2.22: Contribution of salinity and water composition to wettability alteration in carbonates. Figure from Mahani et al. (2017).

Mahani et al. (2015) performed contact angle measurements of oil droplets while exposing them to brines of different salinity. Artificial patches made of crushed limestone and

dolomite material were used as carbonate surfaces for the experiments. The contact angle measurements showed decreasing trend both for limestone and dolomite patches when oil droplets were introduced to SW after being exposed to FW for 40 hours (see Figure 2.23).

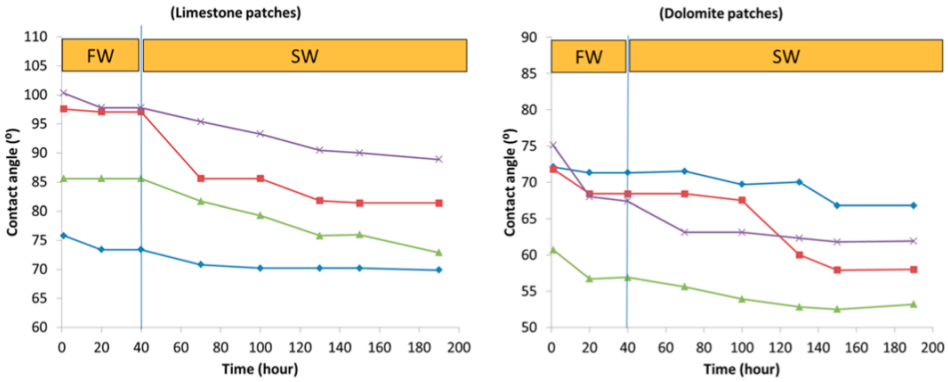

Figure 2.23: Contact angle measurement of oil drops on limestone and dolomite patches under formation water and seawater. Figure from Mahani et al. (2015).

Figure 2.24 visualizes the contact angle change of the oil droplet deposited on a limestone patch (Mahani et al., 2015). It is seen that contact angle (θ) and the diameter of the oil-limestone contact line (L) decreased as water salinity reduced.

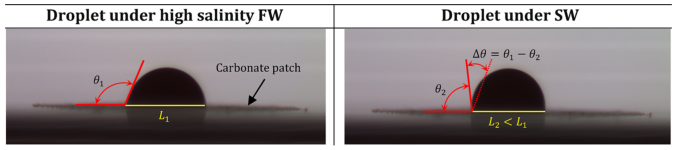

Figure 2.24: Contact angle measurement of the oil droplet on limestone patch under FW and SW. Figure from Mahani et al. (2015).

In another set of contact angle measurements by Mahani et al. (2015), formation water was replaced with 25 times diluted seawater (25dSW). In this case oil droplet deposited on dolomite patches did not show any contact angle changes, while for the droplets on limestone patches significant decrease in contact angle was recorded. However, dissolution of limestone influenced the contact angles which was determined by pH measurements. In order to eliminate rock dissolution effect, 25dSW equilibrated with limestone particles (25dSWEQ) was used to perform one more set of measurements. The contact angle measurement on limestone and dolomite patches showed results comparable to those when the droplets were exposed to 25dSW (see Figure 2.25). In this experiment pH = 9.2 of 25dSWEQ was constant over the time of the experiment indicating that there was no rock dissolution (Mahani et al., 2015).

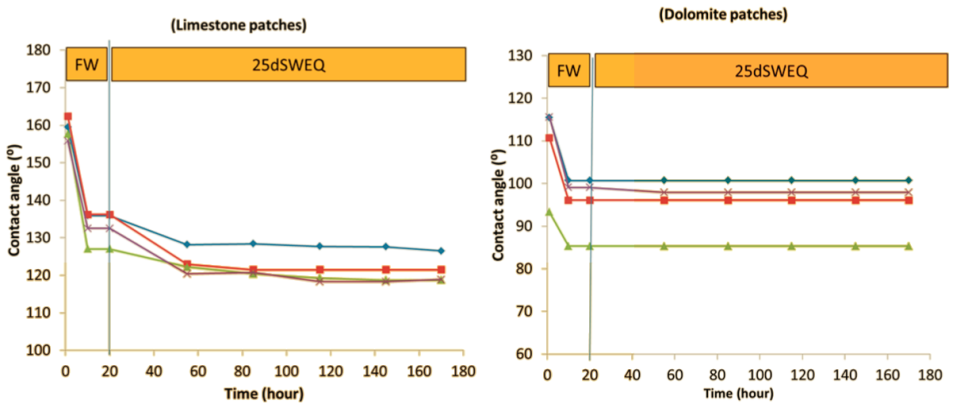

Figure 2.25: Contact angle measurement of oil drops on limestone and dolomite patches under formation water and 25dSWEQ. Figure from Mahani et al. (2015).

Mahani et al. (2015) argue that in their study wettability alteration was caused mainly by changes at rock-brine interface and to a lesser degree at oil-water interface. They emphasize that IFT alone cannot be a reason for the change of contact angles since oil droplets on dolomite patches responded to 25dSWEQ differently from those on limestone.

Zeta potential for oil-brine and carbonate-brine interface at various pH and salinities is illustrated in Figure 2.26 (Mahani et al., 2015). For each plot arrow 1 denotes change of brine salinity and arrow 2 denotes pH increase of the brine. It is seen that zeta potential tends to more positive values as pH increases. Reduction in salinity causes dramatic drop of charge both at oil-brine and rock-brine interface, which leads to increased repulsive forced between rock surface and oil. Consequently, Mahani et al. (2015) conclude that electrostatic repulsion plays a dominant role in wettablity alteration in carbonates.

Comparison of zeta potential measurements on dolomite, calcite, limestone and chalk particles in waters with different salinities at pH 7 is illustrated in Figure 2.27 (Mahani et al., 2017). It is seen that at formation water salinity all carbonate rocks have a positive surface charge which makes the rock oil-wet/mixed wet. Slope change in zeta potential at seawater salinity is an influence of higher concentration of PDIs in seawater tending to regulate the surface charge compared with 25dSW. Calcite shows higher zeta potential at all salinities in comparison with limestone and chalk. On the other hand dolomite shows most positive zeta potential values. This distinction in response to different salinities means that wettability state for various carbonate can be different for the same brine and oil (Mahani et al., 2017). It was related to different surface chemistry and chemical structure of carbonate materials.

Zeta potential showed negative values for limestone and positive for dolomite in the contact angle measurements where 25dSWEQ with pH 9.2 was used. Consequently there was more attractive forces between dolomite patch and the oil drop. This can be a reason for the lack of response of dolomite patches to low salinity water (Mahani et al., 2015).

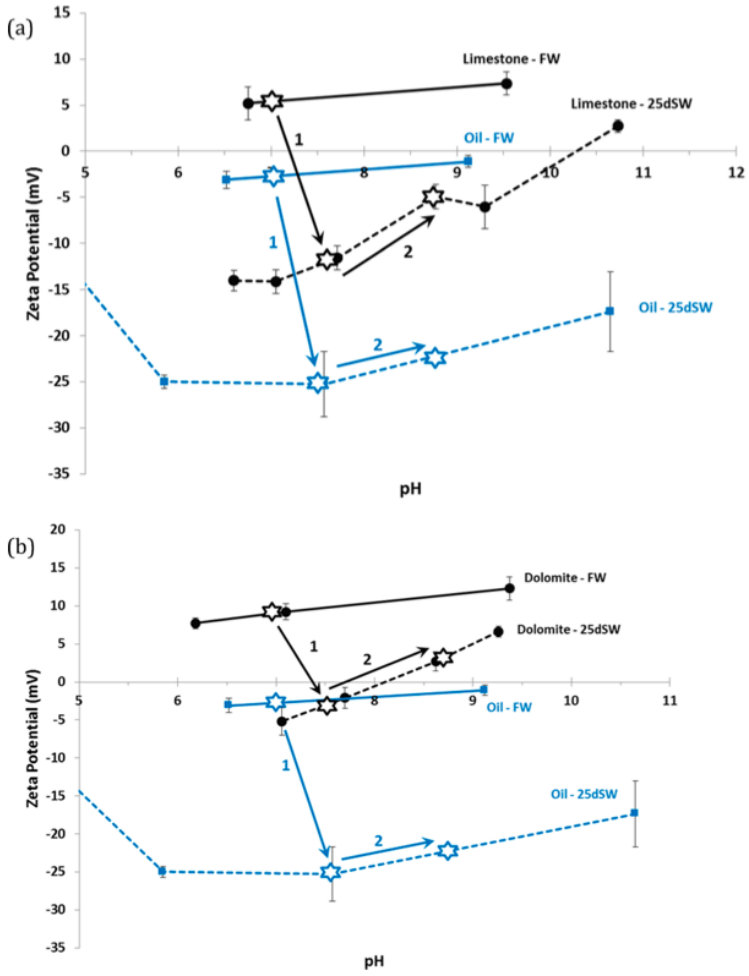

Figure 2.26: Zeta potential as a function of salinity and pH: a) results for limestone and b) results for dolomite. Figure from Mahani et al. (2015).

Mechanism for wettability proposed by Mahani et al. (2017) is summarized in Figure 2.28 as following:

1. Reduced salinity water diffuses into the water film between the oil and rock;
2. EDL expands because of lower water salinity which lead to decrease in zeta-potential values. Contribution of EDL expansion becomes more important at lower salinities;
3. PDIs changes charge to more negative at rock/brine interface and in combination with EDL expansion increases repulsive forces between rock surface and oil-brine interface;
4. Increase in repulsive forces causes recession of oil contact line with rock surface

and wettability change to less oil-wet.

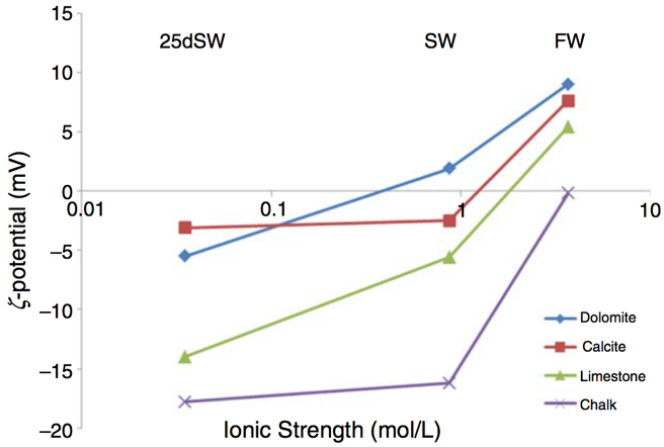

Figure 2.27: Zeta-potential of dolomite, calcite, limestone and chalks in formation water, seawater and 25dSW at pH 7. Figure from Mahani et al. (2017).

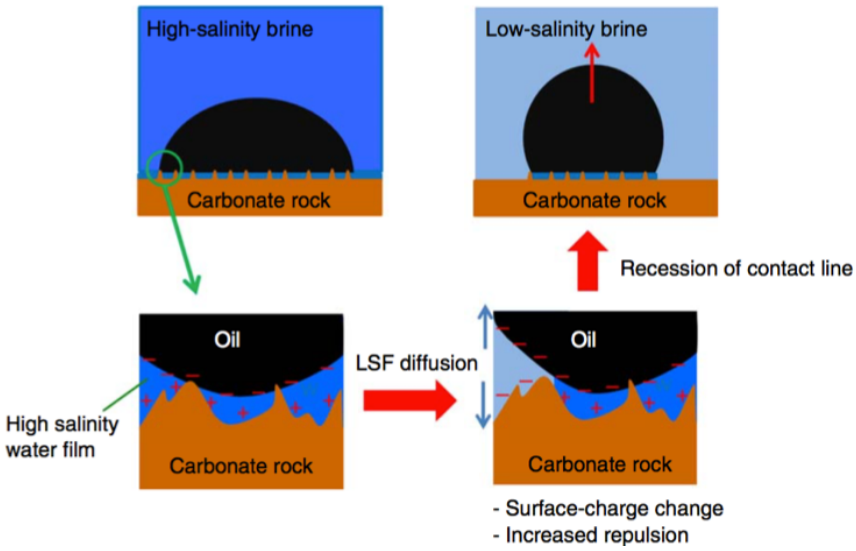

Figure 2.28: Proposed mechanism of wettability alteration by reduced salinity water in carbonates. Figure from Mahani et al. (2017).

2.3 An Overview of Experimental Approaches

It is discussed in section 2.2 that wettability alteration in carbonates is achieved by tuning water ion composition or salinity. Based on a length scale at which wettability alteration is investigated, recent experiments on Low Salinity EOR could be classified as those demonstrating: low salinity effect (LSE) and low salinity recovery (LSR) (Bartels et al., 2019). The LSE is related to a positive response of a system to Low Salinity on a smaller length scale than the core scale, e.g. contact angle change, surface charge change and etc. The LSR is related to incremental oil recovery on a core/field scale upon water salinity or composition change. Although the experiments focusing on the LSE problem give insight in underlying mechanisms of Low Salinity and develop understanding of a crude oil-brine-rock system behavior, they do not show if low salinity EOR leads to incremental recovery on a core/field scale. In essence, LSE for particular rock material does not necessarily mean LSR (Bartels et al., 2019). Experiments on a core/field scale are necessary to confirm positive Low salinity EOR response and demonstrate amount of additional recovery.

The spontaneous imbibition (SI) test is the most commonly used method for qualitative measurement of core wettability (reviewed in Anderson (1986)). The SI method allows to conduct experiments on a large number of core plugs and examine influence of numerous brines on wettability alteration as well as measure incremental oil recovery (in a labour efficient way) (Romanuka et al., 2012). The coreflooding is another method frequently used to study wettability alteration. However, since the SI test is the method used in this thesis, the coreflooding is not discussed in this section.

Two approaches are mainly followed by researchers when SI method is used for wettability studies:

1. Parallel - Each brine is tested on a different core plug (one brine for one plug) (Zhang and Austad, 2006)
2. Serial - Several brines are sequentially tested on the same core plug (Romanuka et al., 2012; Shariatpanahi et al., 2011; Nasralla et al., 2018);

The discussion below is related to SI tests at elevated temperatures since this is a case for most of the experiments (see section 2.2).

In the parallel approach a core plug is exposed to one wettablity modifying (WM) brine only. Core plugs with similar properties are selected for the experiment to be able to compare influence of various WM brines on wettability alteration. Moreover, the core plugs are prepared following the same procedure. The parallel approach allows to keep the core plug under the same conditions throughout the experiment minimizing influence of core handling on results. However, this method requires preparation of a large number of core plugs to statistically show reproducibility of the results. To clarify, reservoir core samples retrieved from different depth might show significantly different response to the same imbibing fluid (Romanuka et al., 2012).

The serial approach allows to expose a core plug to several WM brines sequentially to scrutinize their potential for wettability alteration. This is an advantage if there is a lack of

core material. On the other hand, this method might lead to uncertainty in results due to an experimental protocol being followed. To clarify, in the serial approach a core plug is left to imbibe in a formation water at elevated temperature first. Once oil recovery plateau is reached the SI test is interrupted. The imbibition cell (Amott cell) is removed from the heating cabinet and formation water is replaced by WM brine at ambient conditions. Afterwards the Amott cell is placed back into the heating cabinet and experiment is resumed. This procedure involves exposure of a core plug to air, thermal contraction and further expansion of a core matrix and fluids. At this point it is important to highlight that for experiments at high temperatures (around 100°C and higher) a system is pressurized to prevent fluids from vaporization (Romanuka et al., 2012; Zhang et al., 2007). Therefore, Amott cell is depressurized in order to replace one brine with another. Considering aforementioned plug handling, one might argue that redistribution of fluids in the core plug happens right before WM brine is tested and additional oil production is experimental artefact rather than LSR.

Chapter 3

Theory

This chapter gives an information about the Electric Double Layer (EDL) theory, which describes behaviour of ions in the vicinity of a charged surface and explains existence of electric field in the solution. The chapter is written based on the following sources: Han (2002) and Butt et al. (2003).

3.1 Electric Double Layer Theory

When the solids get in touch with water, their surface becomes charged. The reason behind this stands for the fact that water has high dielectric constant, and is considered as a good solvent for ions. Adsorption of ions to or their dissociation from a surface is one of the causes of a charged surface. Therefore, when a solid is immersed into the water solution, oppositely charged ions (also called counter-ions) are attracted to the solid-liquid interface in order to make the overall charge neutral. First, the layer of static counter-ions bound to the surface, known as a Stern layer, is formed. Some additional counter-ions are attracted by the charged surface, but they are repelled by the Stern layer and keep floating close to the interface, resulting in equilibrium of counter-ions known as tne diffuse layer. Similarly, co-ions inside of the diffuse layer are repelled by the solid. Concentration of co-ions in the diffuse layer is increasing with the distance from the surface until electroneutrality is reached. Hence, electrical potential distribution is created in the solution close to the solid. The charge density at any given point from the solid surface is the difference in the concentration of counter- and co-ions. The charge density is zero in the bulk solution, where electroneutrality is reached. Schematic of EDL is depicted in Figure 3.1

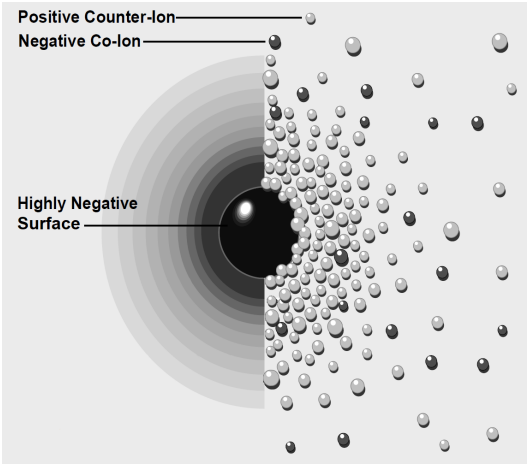

Figure 3.1: Two views of EDL visualization. The left view shows the charge density distribution around the charged solid. The right view shows the concentration of co- and counter-ions around the charged solid. Figure adapted from Zeta Meter Inc (2018).

3.1.1 Gouy - Chapman Model

Electric potential distribution as function of the distance from the charged surface was described by Guoy and Chapman. Their model does not consider the molecular nature of the solvent. Moreover, the solvent is treated as dielectric continuum with continuous charge distribution.

Charge density and electric potential distribution in solution can be described by the Poisson equation:

$$\nabla^2\psi = \frac{\partial^2\psi}{\partial x^2} + \frac{\partial^2\psi}{\partial y^2} + \frac{\partial^2\psi}{\partial y^2} = -\frac{\rho_e}{\epsilon\epsilon_0} \tag{3.1}$$

where

$$\begin{aligned} \psi &= \text{electric potential} & [V] \\ \rho_e &= \text{charge density} & [\frac{C}{m^3}] \\ \epsilon &= \text{dielectric permittivity} & [-] \\ \epsilon_0 &= \text{vacuum permittivity} & [\frac{F}{m}] \end{aligned}$$

For a one dimensional situation of infinite planar surface where the potential cannot change in the y and z directions, Equation 3.1 can be simplified to represent charge distribution along the x-coordinate:

$$\frac{\partial^2\psi}{\partial x^2} = -\frac{\rho_e}{\epsilon\epsilon_0} \tag{3.2}$$

The charge density is a total amount of charges per cubic meter:

$$\rho_e = \sum c_i z_i e \tag{3.3}$$

where

c_i = local concentration of i^{th} species of ions $\quad [\frac{\textit{number of ions}}{m^3}]$

z_i = valence of ions $\quad [-]$

e = the electronic charge $\quad [-]$

Spacial distribution of ions changes with distance from the solid-liquid interface. From Figure 3.1 it is seen that next to the interface there are not many co-ions. On the other hand it is expected that concentration of counter-ions decreases with the distance from the interface. Therefore, local concentration of ions is a function of distance. Local concentration of any particular ion species can be shown by Boltzmann distribution:

$$c_i = c_i^0 \exp(-\frac{z_i e \psi}{k_B T}) \tag{3.4}$$

where

c_i^0 = concentration of i^{th} species of ions in the bulk solution $\quad [\frac{\textit{number of ions}}{m^3}]$

k_B = Boltzmann constant $\quad [-]$

T = Temperature of the system $\quad [K]$

The differential equation of the potential distribution is obtained by substituting Equation 3.3 and Equation 3.4 into Equation 3.2:

$$\frac{\partial^2 \psi}{\partial x^2} = -\sum \frac{z_i e}{\epsilon \epsilon_0} \exp(-\frac{z_i e \psi}{k_B T}) \tag{3.5}$$

Equation 3.5 is easily solved for the low potential case. Low potential means that $z_i e|\psi| < k_B T$. In that case $\exp(-\frac{z_i e \psi}{k_B T})$ can be replaced by $1 - \frac{z_i e \psi}{k_B T}$. Boundary conditions are applied accepting that there is charge neutrality in bulk solution $\psi(x \to \infty) = 0$ and at the surface the potential is equal to surface potential $\psi(x = 0) = \psi_0$. Therefore, the solution for Equation 3.5 is as following:

$$\psi = \psi_0 \exp(-kx) \tag{3.6}$$

For a monovalent salt solution:

$$k = \sqrt{\frac{2 c_0 e^2}{\epsilon \epsilon_0 k_B T}} \tag{3.7}$$

where

c_0 = bulk concentration of a monovalent salt $\quad [\frac{L}{mol}]$

For solution with higher valency ions present:

$$k = \sqrt{\frac{e^2}{\epsilon\epsilon_0 k_B T} \sum c_i^0 z_i^2} \tag{3.8}$$

From Equation 3.6 it is seen that the potential decreases exponentially with the distance from solid surface. Low potential case is valid for applications when potential is not higher than 80 mV.

3.1.2 Debye Length

The Debye length shows decay length of the potential or in other words the thickness of EDL. The Debye Length is given by $\lambda_D = k^{-1}$. The higher is the salinity of the water the better surface charge is electrically screened, because there are more ions in the solution. Therefore, the thickness of the EDL decreases dramatically as the salinity of the water increases. This phenomenon is also known as double-layer compression. The Debye length for monovalent salt solution at 25°C is:

$$\lambda_D = \frac{3.04 \text{ Å}}{\sqrt{c_0}} \tag{3.9}$$

where

$$\text{Å} = \text{angstrom, unit of length} \qquad [10^{-10}\ m]$$

The Debye length is a reverse of Equation 3.8 for divalent salt solution. Figure 3.2 depicts effect of salinity on the potential with increasing distance. Exponential decrease of potential becomes steeper with increasing salinity.

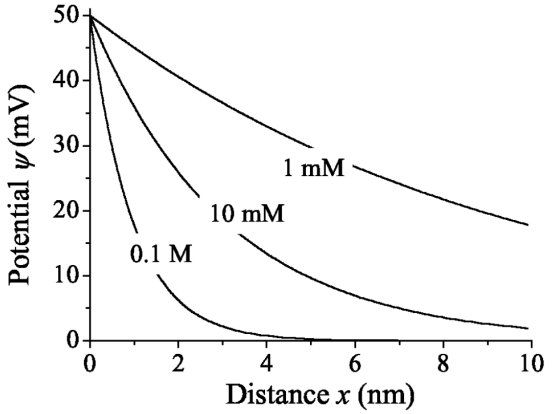

Figure 3.2: Potential distribution for different monovalent salt concentrations. Figure from Butt et al. (2003).

3.1.3 Stern Layer and Zeta Potential

Specific ions are attracted into the EDL and adsorbed to the surface due to the surface nature. These ions are affected by interaction with the surface and create a layer of immobile ions on the solid surface. However the Gouy-Chapman model is valid only if indifferent ions considered to be present in the solution. These ions enter and leave double layer as long as electroneutrality is kept and do not adsorb irreversibly to the solid surface. Stern theory takes into account the layer of static ions adsorbed to the surface. Therefore, a combination of the Gouy-Chapman model and Stern theory describes the electric double layer in terms of two layers: inner layer of immobile ions, *Stern layer*, and outer layer of mobile ions, *diffuse layer*. A simple version of Stern layer is depicted in Figure 3.3. There is a linear decrease of potential over distance δ from surface to the centre of ions. In some cases not only one, but two or more layer of ions can be adsorbed on to the surface.

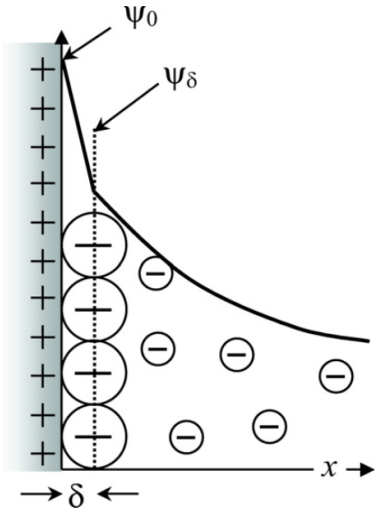

Figure 3.3: Simple version of Stern layer. Figure from Butt et al. (2003).

The plane where the Stern layer ends and diffuse layer starts is referred to as *Shear plane*. The potential at the shear plane is called the zeta potential - ζ (see Figure 3.4). Ions which are able to change zeta potential values are known as potential determining ions (PDIs). Isoelectric point (iep) is the concentration of PDIs at which potential at the shear plane is equal to zero. Point of zero charge (pzc) is the pH of solution at which surface has zero potential.

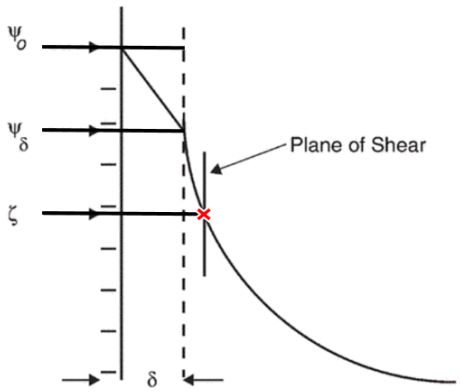

Figure 3.4: Schematic of zeta potential. Figure from Han (2002).

Chapter 4

Methods and Materials

This, chapter describes the new experimental setup designed for the SI tests at elevated temperatures ($<100°C$). Secondly, methods and material used to perform core analysis, and experiments supporting the wettability alteration study are presented herein.

4.1 Experimental Setup

The SI tests were conducted in the heating cabinet at the temperature of 96°C. The serial approach (see section 2.3) was chosen for the study due to the shortage of core material. An experimental setup suitable for high temperatures was specially assembled and tested prior to the experiment. The objective of the setup was to avoid core handling during the SI tests (see section 2.3). Therefore, a system which allows replacement of one imbibing brine with another without interruption of the SI test was developed.

4.1.1 Setup Configurations

Two sets of experiments were conducted during the study. One set scrutinized the effect of salinity, while another set examined the effect of ion composition on wettability alteration. A different approach for brine replacement was developed for each set (the reason is discussed later in this section). Therefore assembled setup has three configurations used for:

- The imbibition test - used for both sets;
- Replacement of high salinity brine with low salinity brine;
- Replacement of brine with another brine of comparable salinity.

Although the SI tests were conducted at 96 °C, imbibition cells (Amott cells) were not pressurized because of characteristics of the assembled setup. All lines used in the setup are made of Polytetrafluoroethylene (PTFE).

The imbibition test

The setup layout during the imbibition test is illustrated in Figure 4.4. Initially, a brine free imbibition cell with a core plug inside is filled up at a rate of 5 ml/min using a peristaltic pump through water lines. This allows mild submersion of a core plug into brine. Oil recovered during SI test is collected at ambient conditions into graduated glass tubes outside the oven through oil collection lines. Brine is pumped into a cell for a short period of time (2-3 minutes) every 24 hours at a rate of 5 ml/min in order to move produced oil from the cell into the graduated tube. Occasionally negligible amount of oil is retained in the lines. All flow directions are shown in Figure 4.4 with red arrows. The length of the water (brine) lines (1.5 meters) was estimated to be sufficient to heat up brine to 96°C at the moment it enters an imbibition cell (see section 4.1.2).

When static, brine inside the water lines gets vaporized at 96°C after a period of time. Whenever oil is moved from a cell to a graduated tube, the vapour is flushed through vapour lines beforehand. Therefore, entry of vapour into the cell and its contact with a core plug, which can cause detachment of oil droplets from the core surface, is prevented. The tee valve switching flow direction from ”Amott cell” to ”vapour line” and back is manually operated, hence requires opening of a heating cabinet for a short time. Moreover, brine entering the oil collection lines, when oil is moved, gets vaporised over time as well. This vapour accumulates in a graduated glass tube and eventually pushes liquids out of it. To prevent this from happening, a graduated tube with a pipette filler was utilized which allows adjusting the level of liquid in the tube. Over time graduated glass tubes become more oil wet, which brings uncertainty to the readings of the recovery as the oil spreads over the glass. Hence, the readings are taken before adjusting the level in the graduated tube and pumping the brine into the cell (to move produced oil from the cell). This gives time to oil (produced one day before) to flow down the glass surface and accumulate, which allows to perform accurate readings.

Replacement of high salinity brine with low salinity brine

The configuration of the setup illustrated in Figure 4.5 was used in the set of experiments dedicated to the influence of brine salinity on wettability alteration. The idea behind the replacement of high salinity brine with low salinity brine is the gravity segregation of liquids. It was tested and shown in Figure 4.1a that there is clear segregation between brines because of the density difference when 10dSSW displaces SSW from the imbibition cell at a rate of 5 ml/min. In Figure 4.1a 10dSSW (colored to blue) is pumped from the top of the cell to displace SSW. Replacement of SFW by SSW was also tested and showed the same behavior due to the fact that the density difference between these liquids is even higher. The densities of SFW, SSW, 10dSSW used in this set of experiments are shown

in Table B.1. When this approach was tested at 96°C it was found out that the brine slowly vaporizes in the thin graduated tube of the Amott cell lowering the brine level in the cell (see Figure 4.1b), however, this does not affect the brine displacement process. In the cases if a thin graduated tube of the Amott cell was completely free of brine because of vaporisation, a small volume (max 10 ml) of the heavy brine was pumped from the bottom of the cell to displace the vapour from the graduated tube. Afterward, the brine displacement process is resumed.

To perform the replacement of high salinity brine with low salinity brine, the components of the setup located outside the oven has to be rearranged from what is depicted in Figure 4.4. The peristaltic pump is disconnected from the lines at the bottom of Amott cells and connected to the lines on the top. When this manipulation is executed, the pump hose is drained to remove high salinity brine from it. At this point, the pump hose is full of air, which is flushed out through "Air control system" (see Figure 4.5) before low salinity brine is pumped into the Amott cell. The low salinity brine is pumped into the cell at a rate of 5 ml/min. All flow directions are shown in Figure 4.5 with red arrows. The brine displaced from the cell flows through ohmmeter which verifies the complete change of brine in the cell qualitatively by means of resistivity. Brine can be replaced only in one cell at a time.

Replacement of brine with another brine of comparable salinity

The configuration of the setup illustrated in Figure 4.6 was used in the set of experiments dedicated to the influence of brine ion composition on wettability alteration. In this set of experiments used brines have comparable salinity and same density (see Figure 2.10). Total dissolved solids slightly differs among brines which allows confirming complete brine displacement by means of resistivity, however, displacement front is not as sharp as observed for brines of different salinities. Because of the same density very slow mixing of brine happens at the displacement front. Experimentally it was found out that slight mixing occurs when displacing from bottom to top at the rate of 5 ml/min. Figure 4.1c depicts the displacement of SSW by SSW2SO4 (synthetic seawater with doubled sulfate content) from bottom to top at the rate of 5 ml/min. It was determined by means of resistivity that two cell volumes have to be pumped to completely replace one brine with another.

Displacement of brine is performed through water lines connected to the top of the imbibition cell. An ohmmeter is connected to brine lines in order to measure the resistivity of displaced brine. Brine lines are connected to graduated glass tubes to collect oil which could be produced while brine replacement process. Brine can be replaced only in one cell at a time.

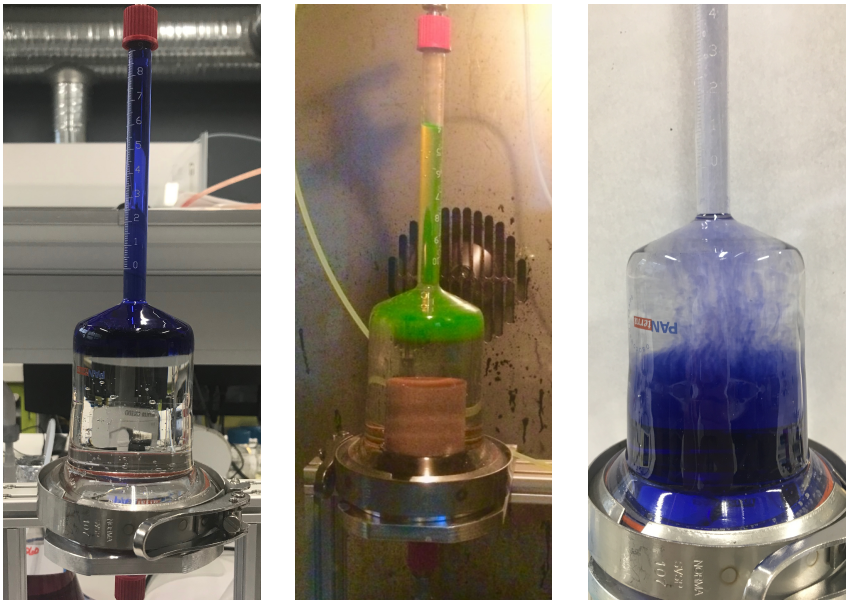

(a) **(b)** **(c)**

Figure 4.1: a) replacement of SSW with 10dSSW (blue) at a room temperature; b) replacement of SSW with 10dSSW (green) at 96°C; c) replacement of SSW by SSW2SO4 (blue).

4.1.2 Setup Components

Imbibition cells

The High Temperature (HT) Amott cells manufactured by PanTerra were used as a part of the setup. These Amott cells are developed to perform at high temperatures and suitable both for drainage and imbibition tests. The components comprising a HT Amott cell are illustrated in Figure 4.2.

Ohmmeter

The used ohmmeter consists of clamps connected to steel connections of a PTFE line and a receiver, displaying the measurements. A distance between the steel connections is approximately 10 cm. The resistivity is measured over this distance. The ohmmeter is very sensitive to the temperature variations in the room and to the length of a line between the heating cabinet and the ohmmeter. Therefore it was possible to use it only for qualitative check of brine replacement.

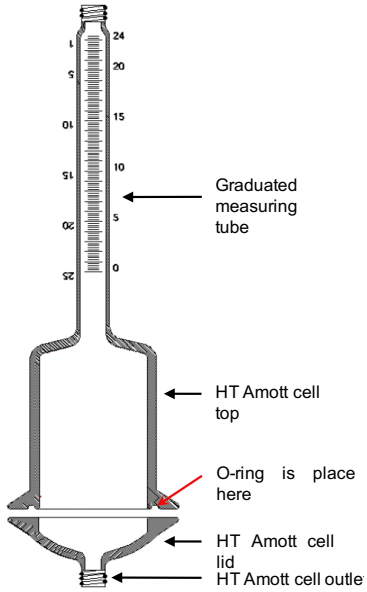

Figure 4.2: Parts comprising HT Amott cell. Figure adapted from PanTerra Geoconsultants (2018).

Pump

The peristaltic pump (see Figure 4.3a) was used because of the availability of the equipment. On the other hand, this type of pump is portable and gives a possibility to rearrange parts of the setup fast. Moreover, the pump components do not contact with highly saline brines, hence does not degrade due to the contact with salt. This makes the pump robust and stable for the applications when aggressive liquids are used.

Brine lines

A line length of 1.5 meters and higher was experimentally estimated to be enough to heat up a brine to 96°C while the brine is flowing inside of the line. PTFE lines of various lengths (1, 1.5, 3 and 5 meters) were tested.

A line was placed into a heating cabinet at 96°C. Synthetic formation water was pumped through a line and the temperature of the brine was measured at the outlet using digital thermometer. Since the outlet of the line is outside the heating cabinet (at a room temperature), there was a heat loss before the temperature measurement point. Therefore, the measured temperature had never reached 96°C. However, starting from the length of 1.5 meters and longer the temperature at the outlet always converged to 75-81°C. Based on the measurements, it is believed that starting from the length of 1.5 meters the temperature of brine reaches 96°C in the heating cabinet. All brine lines used in the setup were 1.7 meters and longer.

Core stand

Because of the spherically curved shape of the HT Amott cell lid, the core plug placed in a vertical position blocks the the outlet of the cell and prevents flow of brine. Therefore, special core stand was designed. The stand allows brine to flow through the openings in the body of the stand. Figure 4.3b depicts the stand with a core plug on top of it inside of the Amott cell lid. The top of the stand is a solid platform, therefore a core plug has a limited contact with imbibing brine on the bottom face.

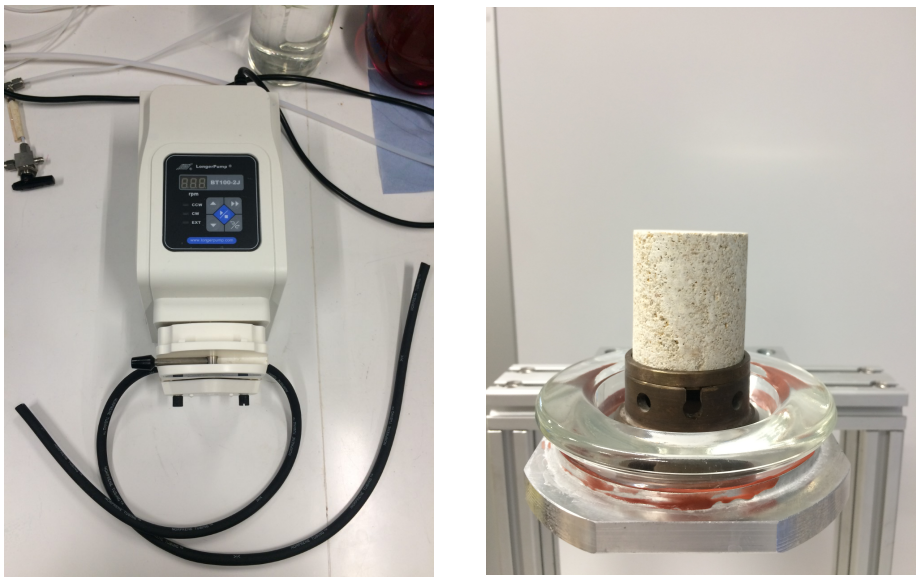

(a) **(b)**

Figure 4.3: a) The peristaltic pump used for the setup; b) the core stand with the core plug on top of it.

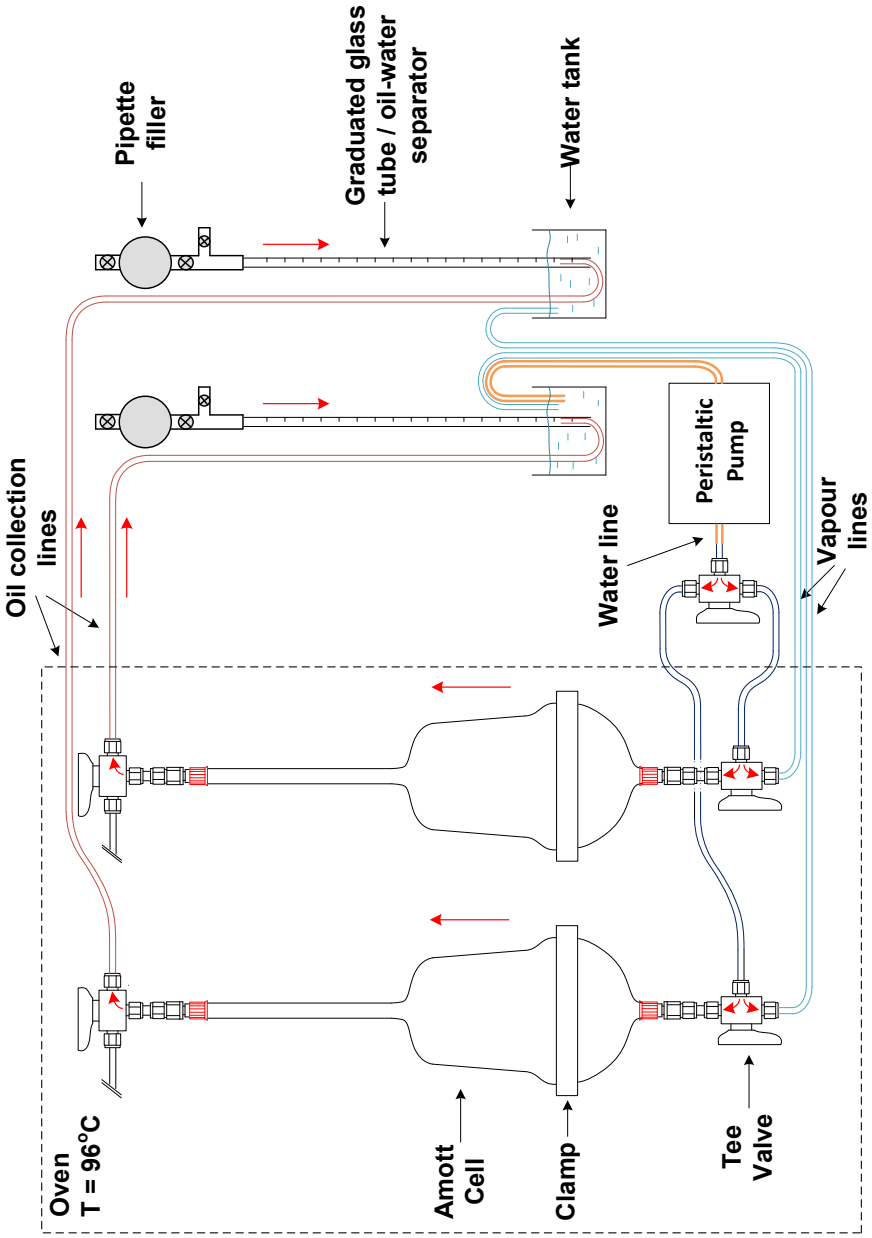

Figure 4.4: The configuration of the setup during the SI test.

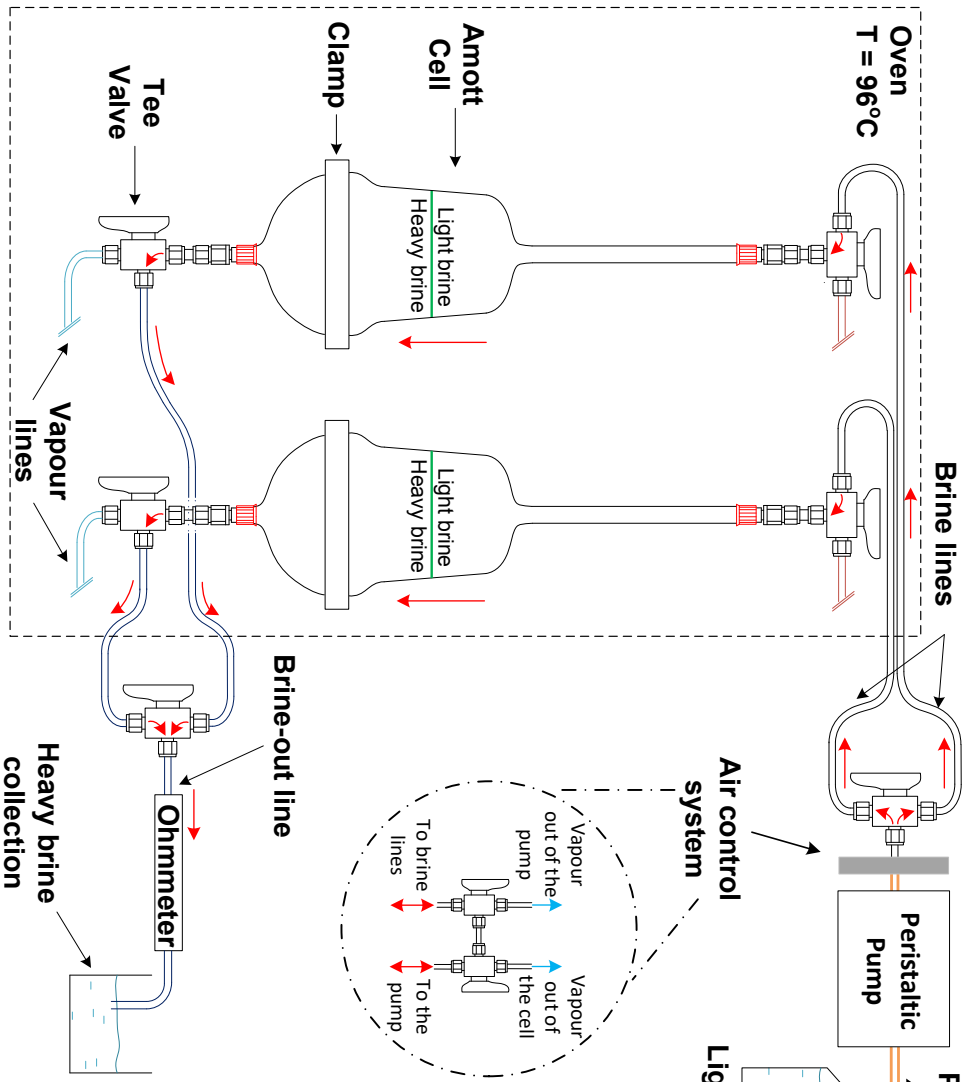

Figure 4.5: The configuration of the setup during the replacement of high salinity brine with low salinity brine.

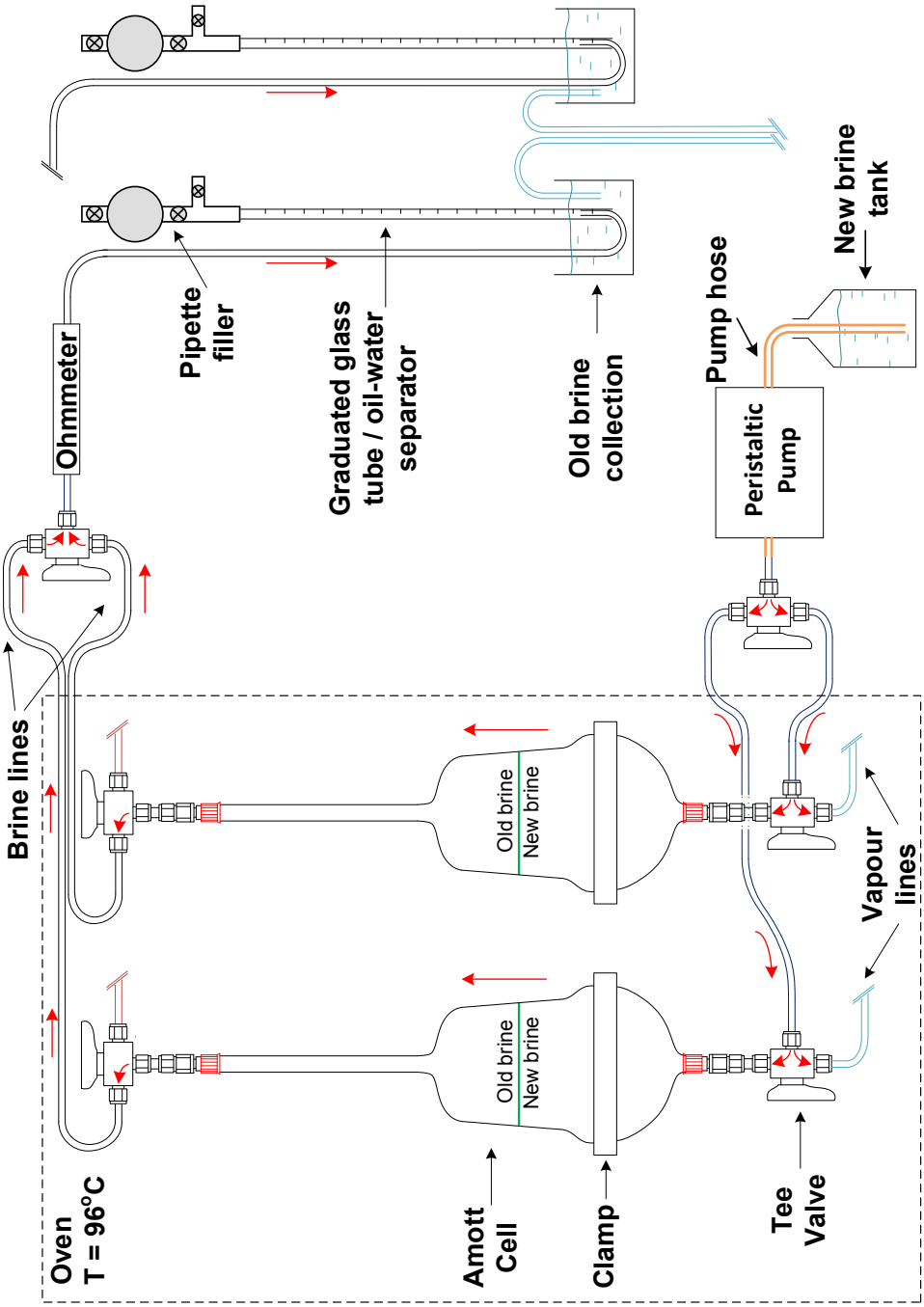

Figure 4.6: The configuration of the setup during the replacement of brine with another brine of comparable salinity.

4.2 Liquids Preparation

4.2.1 Brines

Synthetic brines were prepared for the study using (DI) deionized water and laboratory salts. The salts and amounts used to prepare the brines considered in the experiments are presented in Table 4.1. The ion composition of synthetic formation water (SFW) and synthetic seawater were provided by Equinor. Ten times diluted synthetic seawater water (10dSSW) was prepared by mixing SSW with DI water. SSW2SO4 and SSW4SO4 are synthetic seawater enriched with two and four times the sulfate concentration respectively. The ionic strength of SSW2SO4 and SSW4SO4 was kept constant by adjusting concentration of NaCl. A magnetic stirrer was used for stirring all solutions. All SFW solutions were prepared from DI water degassed beforehand by stirring at high temperature. However, this brine degassing approach was found inconsistent when preparing other solutions later. The rest of the solutions were vacuum degassed, the latest 2 hours before use, for 45 minutes while stirring.

Table 4.1: Amount of salt dissolved in water.

Salt [g/l]	SFW	SSW	10dSSW	SSW2SO4	SSW4SO4
$NaCl$	148.521	23.741	2.3741	18.833	9.017
$NaHCO_3$	0	0.194	0.0194	0.194	0.194
Na_2SO_4	0	3.976	0.3976	7.952	15.904
KCl	5.510	0.755	0.0755	0.755	0.755
$MgCl_2x6H_2O$	22.927	10.696	0.10696	10.696	10.696
$CaCl_2x2H_2O$	99.473	1.5	0.15	1.5	1.5
$SrCl_2x6H_2O$	13.338	0.024	0.0024	0.024	0.024

SFW. Sodium chloride was mixed with about 1000 ml of DI water in glass flask A. The solution was stirred for 30 minutes. All other chloride salts were added into glass flask B containing approximately 600 ml of DI water. The solution was stirred for 30 minutes. Content of flask B was poured into flask A. Then flask B was rinsed with a small amount of DI water and added to flask A. Flask A was filled up with DI water up to 2-liter mark. The volume displaced by stir bar was taken into account by adding extra 8 ml of DI water into the solution. The solution was stirred for 30 more minutes right before the core water saturation procedure started.

SSW/SSW2SO4/SSW4SO4. Sodium sulfate was dissolved in about 200 ml of DI water in glass flask A. The solution was warmed up to 50°C while stirring on a magnetic stirrer for 20 minutes. Glass flask B was filled with 600 ml of DI and sodium chloride was dissolve in it. The solution was stirred for 20 minutes. The solution from flask B was poured into flask A. The rest of the salts, in exception with $NaHCO_3$, were mixed with 400 ml of DI water in flask B. The mixture was stirred for 20 minutes. The content of flask A was poured into flask B. Flask A was rinsed with small amount of DI water and added to flask B. Afterward, sodium bicarbonate was added to flask B and the solution was stirred for 10

minutes. Flask B was filled up with DI water up to 1-liter mark. The volume of the stir bar was compensated by adding 8 ml of DI water. The solution was moved from flask B into a 2L glass bottle for degassing.

10dSSW. First, glass flask was filled with 200 ml of SSW and then was filled up to 2-liter mark with DI water. The solution was stirred for 10 minutes. The volume of the stir bar was compensated by adding 8 ml of DI water. The solution was moved from flask B into a 2L glass bottle for degassing.

4.2.2 Oil

Heidrun crude oil was obtained from Equinor. The acid number of the oil is 2.9 mg KOH/g (reported by Equinor).

The oil was filtered through 5 μm filter paper using Büchner funnel to remove particulate matter. Schematic of the filtration process using the Büchner funnel is depicted in Figure 4.7a. The components of the filtration setup are illustrated in Figure 4.7b

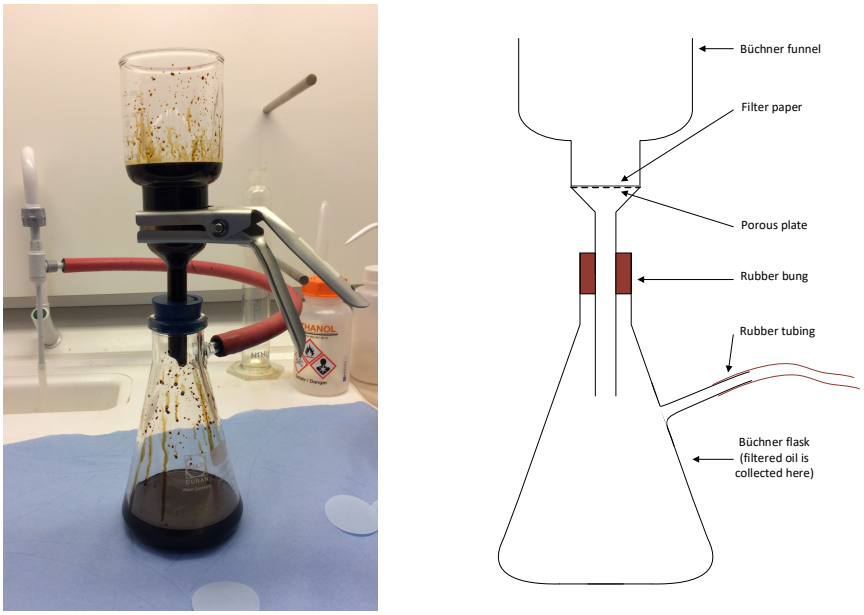

(a) **(b)**

Figure 4.7: a) Filtration process; b) Schematic of filtration setup using Büchner funnel.

The Büchner funnel was connected to the side-arm flask (also called Büchner flask) and placed into the fume hood. A rubber tubing was attached to the side-arm of the Büchner flask to access the suction line which creates a vacuum driving the oil through the filter

paper. Vacuum suction was activated, and oil was poured into the Büchner funnel. Oil flowed through the filter paper and was collected into the Büchner flask.

The oil was degassed at elevated temperature (80°C) for 30 minutes in the fume hood. The oil was stirred using a magnetic stirrer to enhance the degassing process.

4.2.3 Interfacial Tension

Interfacial tension (IFT) measurements for the oil-brine system were executed using KRUSS Drop Shape Analyzer. A pendant drop method was used for the measurements. A hooked (U-shape) needle with an outer diameter of 1.001 mm was submerged into a cell, pre-filled with a brine of interest. The needle was used as a reference for scale calibration. A digital image of a stable pendant drop created on the needle was acquired (see Figure 4.8). Software processes the drop shape (interfacial contour) and fits it into the Young-Laplace equation of capillarity to obtain IFT values. All measurement were performed at room temperature 25°C. However, the temperature in the room varied ± 0.3°C from one IFT test to another. The IFT was taken when a droplet reaches equilibrium.

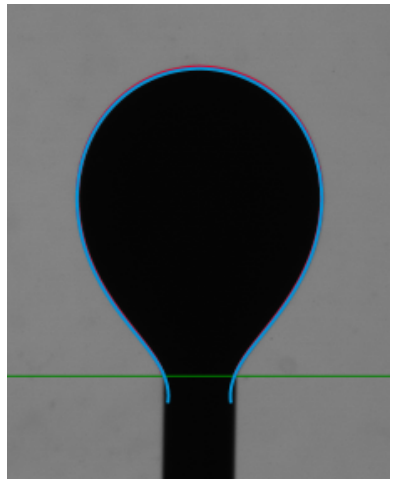

Figure 4.8: A pendant drop on the hooked needle. The green line is the baseline of the area of interest. The blue line is the interfacial contour.

4.3 Core Analysis

4.3.1 Core preparation

Core cutting

Four carbonate core samples from the Ainsa Basin in the Spanish Pyrenees were provided by Equinor for the experiment. Each of the samples had a diameter of approximately 3.70 - 3.82 cm and length of 10 - 13 cm. Optimal operation of Beckman centrifuge, used to establish irreducible water saturation (see subsection 4.5.2), requires certain dimensions of the core plug: a maximum length of 4.6 cm and a maximum diameter of 3.81 cm. A precision circular saw was used to cut the core samples in order to obtain the core plugs of the required length. The core samples were rotated while cutting to prevent chip off at the cutting plane. Distilled water was used for cooling while cutting.

Core Dimensions

In order to account for deviations from the desired dimensions after core cutting, and to obtain an accurate bulk volume of the cores, length, and diameter of the core plugs were measured using digital Vernier caliper. To mitigate variation of the diameter along the core plugs, measurements were taken at both ends and in the middle of the core plugs. Three measurements of the length for each core plug were obtained by rotating them while measuring. Averages of the measurements were used for calculations. Cross-sectional area of each core plug was found using Equation 4.1:

$$A = \frac{\pi d^2}{4} \tag{4.1}$$

$A =$ cross-sectional area of the core plug $[cm^2]$
$d =$ average diameter of the core plug $[cm]$

Bulk volume of each core plug was computed using Equation 4.2:

$$V_{bulk} = A * L \tag{4.2}$$

$V_{bulk} =$ bulk volume of the core plug $[cm^3]$
$L =$ average length of the core plug $[cm]$

Core Cleaning

Although the core samples obtained for the experiment are the outcrop material, cleaning with methanol using Soxhlet extractor was performed to remove dust from cutting or any foreign particles. After the cleaning process was finished, the core plugs were dried in the heating cabinet at 60°C until the weight of the plugs became constant.

4.3.2 Porosity Measurements

Helium porosimeter and liquid saturation methods were used to determine effective porosity of the cores.

Helium Porosimeter Method

Porosity measurement using helium porosimeter is based on an estimation of reference volume of an empty chamber and volume of chamber containing core plug. The difference between the two volumes is the grain volume of a core sample (Equation 4.3). Schematic diagram of helium porosimeter is illustrated in Figure 4.9.

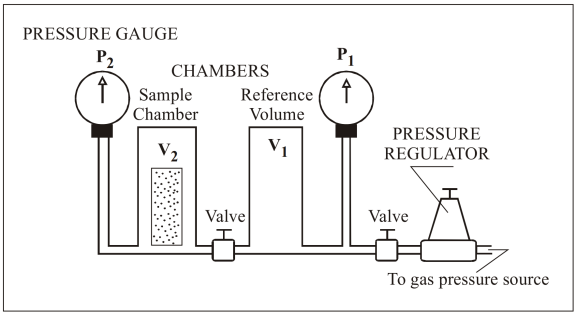

Figure 4.9: Schematic diagram of helium porosimeter apparatus. Diagram from Torsæter and Abtahi (2003).

$$V_{grain} = V_1 - V_2 \tag{4.3}$$

where

$$\begin{aligned} V_{grain} &= \text{total grain volume of the sample} && [cm^3] \\ V_1 &= \text{volume of matrix cup without a core plug} && [cm^3] \\ V_2 &= \text{volume of matrix cup with a core plug} && [cm^3] \end{aligned}$$

Pore volumes of the core samples were found using Equation 4.4:

$$V_{pore} = V_{bulk} - V_{grain} \tag{4.4}$$

where

$$V_{pore} = \text{pore volume of a core plug} \qquad [cm^3]$$

Effective porosity in percentage was calculated using Equation 4.5 below:

$$\phi_e = \frac{V_{pore}}{V_{bulk}} * 100 \tag{4.5}$$

where

$$\phi_e = \text{effective porosity} \qquad [\%]$$

Liquid Saturation Method

Effective porosity determination by means of saturation of a core with liquid is known as liquid saturation method. The core samples were weighed before and after being saturated with synthetic formation water (see subsection 4.5.1). The pore volume of the cores was computed using Equation 4.6 below, while effective porosity using Equation 4.5.

$$V_{pore} = \frac{W_{wet} - W_{dry}}{\rho_w} \tag{4.6}$$

where

$$\begin{aligned} W_{wet} &= \text{weight of the core saturated with water} && [cm^3] \\ W_{dry} &= \text{weight of the dry core} && [g] \\ \rho_w &= \text{density of synthetic formation water} && [g/cm^3] \end{aligned}$$

4.3.3 Grain Density

The matrix grain density was computed (Equation 4.7) using grain volume and dry weight obtained from Helium Porosimeter and Liquid Saturation methods respectively.

$$\rho_{grain} = \frac{W_{dry}}{V_{grain}} \tag{4.7}$$

where

$$\rho_{grain} = \text{matrix grain density} \qquad [g/cm^3]$$

4.3.4 Permeability Measurements

Liquid permeability of the cores was found by applying Klinkenberg correction (Klinkenberg, 1941) to air permeability measurements. Constant head permeameter in combination with Hassler type core holder was used to determine air permeability of the cores. Schematic of constant head permeameter is shown in Figure 4.10.

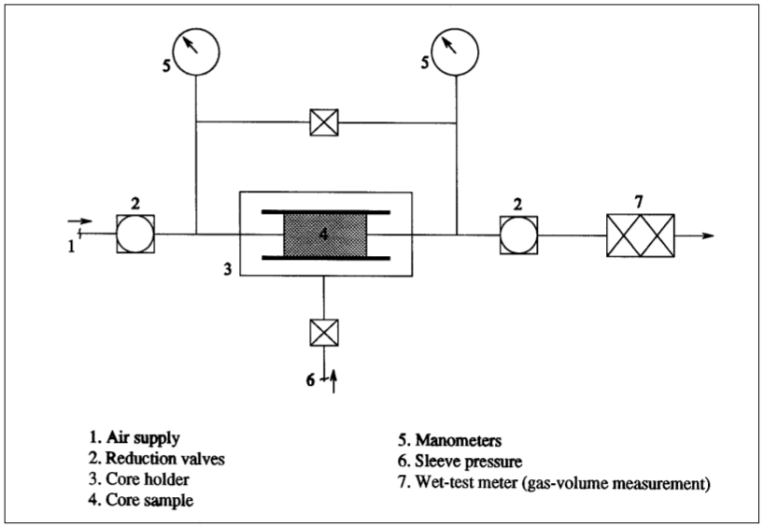

Figure 4.10: Schematic diagram of constant head permeameter. Diagram from Torsæter and Abtahi (2003).

Four permeability tests were conducted at several upstream and downstream pressures keeping the difference between them constant at 0.2 bar. Equation 4.8 was used to compute air permeability for each of the tests.

$$k_g = \frac{2 * Q * \mu * L * P_{atm}}{A * (P_1^2 - P_2^2)} \tag{4.8}$$

where

$$\begin{aligned} k_g &= \text{air permeability} && [D] \\ Q &= \text{flow rate} && [ml/s] \\ \mu &= \text{air viscosity} && [cP] \\ P_{atm} &= \text{atmospheric pressure} && [atm] \\ P_1 &= \text{upstream pressure} && [bar] \\ P_2 &= \text{downstream pressure} && [bar] \end{aligned}$$

Klinkenberg (1941) deduced that air permeability is related to liquid permeability by Equation 4.9 below:

$$k_g = k_L(1 + \frac{b}{P_m}) \tag{4.9}$$

where

$$\begin{aligned} P_m &= \text{mean pressure} && [atm] \\ b &= \text{Klinkenberg constant} && [-] \end{aligned}$$

With the mean pressure computed using Equation 4.10:

$$P_m = \frac{P_1 + P_2}{2} \tag{4.10}$$

4.4 Zeta Potential Measurements

Zeta potential measurements were performed on limestone aqueous suspensions using ZetaSizer Nano-ZS (Ainsa carbonate is classified as limestone in subsection 5.2.6). The instrument measures electrophoretic mobility of particles and infers zeta potential from it using Equation 4.11 known as Henry's equation:

$$U_e = \frac{2\epsilon\zeta f(Ka)}{3\eta} \tag{4.11}$$

where

$$\begin{aligned} U_e &= \text{electrophoretic mobility} & [\frac{m^2}{Vs}] \\ \zeta &= \text{zeta potential} & [mV] \\ f(ka) &= \text{Henry's function} & [-] \\ \eta &= \text{dynamic viscosity of a liquid} & [mPa * s] \end{aligned}$$

For the particle size of 0.2 microns and larger $f(Ka)$ is 1.5, which is also known as Smoluchowski approximation (Malvern Instruments Ltd, 2013). Dielectric constant as a function of salinity was approximated from the data reported by Buchner et al. (1999). Viscosity values are reported in Appendix B.

The limestone rock was crushed to the powder of about 10-micron particle size using grinding rings made of agate in a Vibratory Disc Mill. The limestone aqueous suspensions were prepared by mixing 10 g of limestone powder with 90 g of brine, which makes up 1 wt%. The suspensions were stirred using magnetic stirrer for about 18 hours. Then the suspensions were left to rest for 2 hours to equilibrate. The supernatant was used for zeta potential measurements. Zeta potential is selected as the average value of 20-30 measurements. Each measurement had 15-100 runs. Zeta potential measurements for limestone suspensions in all brines considered in the SI test was performed at 25°C. A pH meter was used to measure pH of the brines at 25°C.

Initially, powder of 63-micron particle size was used to prepare aqueous suspensions. However, particles were falling out of suspension while performing the measurements and this led to inconsistent results.

4.5 Saturation of Core Plugs

First, Ainsa carbonate core plugs were saturated with SFW. Afterward, the cores plugs were drained by Heidrun crude oil.

4.5.1 Water Saturation

Vacuum pump apparatus depicted in Figure 4.11 was used to saturate dry core plugs with SFW. Evacuation of air and subsequent submersion of the cores into the SFW intensifies imbibition of liquid into the cores. This is achieved by the increased difference between pressure of water and reduced air pressure in the core.

All core plugs used for spontaneous imbibition test were placed into the empty plastic beaker inside of the vacuum chamber (also referred to as evacuator). The vacuum pump was started to lower pressure in the evacuator to about 0.1 bar. Once the pressure was lowered, the plastic beaker was filled with SFW until the core plugs were fully immersed into the water. The core plugs were left in the evacuator for 2 hours, while vacuum pump running. Afterward, the plastic beaker was extracted from the evacuator and the cores remained fully submerged into the water until the drainage procedure began.

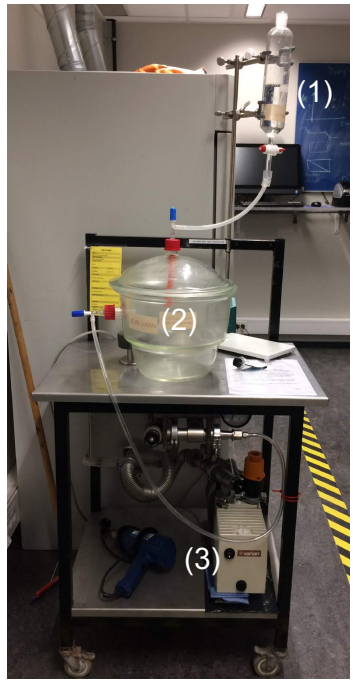

Figure 4.11: Schematic of vacuum pump apparatus: 1) Glass tank containing formation water; 2) evacuator; 3) vacuum pump.

4.5.2 Oil Saturation

The Beckman centrifuge was utilized to saturate the core plugs with oil and establish the irreducible water saturation. Figure 4.12 illustrates the drainage process using the centrifuge. In the oil-water drainage system, a core sample fully saturated with water is immersed into the oil in the centrifuge drainage cup. The drainage process is executed by rotation of the centrifuge drainage cup at a high rotational speed. The centrifugal force caused by rotation pushes oil into the core displacing water and establishing irreducible water saturation.

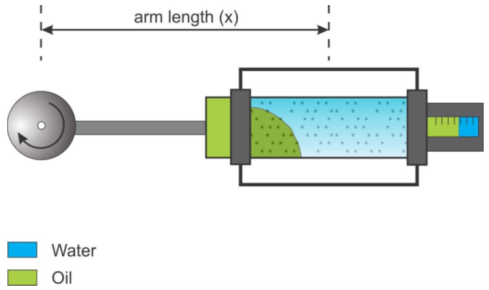

Figure 4.12: Fluid displacement by drainage process. Diagram from Weatherford International (2013).

The procedure below describes the assembly of a drainage cup for one core plug. The same procedure was used to assemble the cups for all core plugs. Schematic of a drainage cup assembly is illustrated in Figure 4.13a.

Starting volume of 8 ml of SFW was added into the calibrated polycarbonate receiving tube. Afterward, the tube was filled up with crude oil. The sample tube and calibrated polycarbonate receiving tube were connected to each other. The rubber cushion and fluid distributor were set into the sample tube. The core was placed into the sample tube and oil was added into the tube until the core was fully submerged into the oil. The sealing lid was screwed into the sample tube. The drainage cup is set into the aluminium bucket before mounting it into the centrifuge rotor.

For safe and correct operation of the centrifuge following requirements has to be met:

- The centrifuge rotor has three cup sockets and it is required that three drainage cups are installed into the rotor;
- All three drainage cups mounted in the centrifuge rotor has to have equal weight (+/- 0.08 g);
- If any bucket does not meet a weight requirement, small pieces of lead or the oil can be added into the bucket.

Two pairs of core plugs were saturated with oil, hence there were two centrifuge runs, A dummy core plug was placed into the third drainage cup at each of the centrifuge runs

to fulfill the requirements discussed above. Figure 4.13b depicts the drainage cups fully assembled, but sealing lids, which are in front of the cups. One can see the dummy core plug inside of drainage cup in the middle (DI water was used instead of crude oil for this drainage cup assembly). The aluminium buckets are behind the drainage cups.

The cores were centrifuged for 10 hours at 5000 rev/min. Water displaced from the core plug is collected in the calibrated polycarbonate receiving tube. The tube was removed from the drainage cup assembly and the content was poured into the burette to find the volume of produced water.

The irreducible water saturation was calculated using Equation 4.12. Volume of produced water must be measured at the same temperature as the one during centrifuging. The irreducible water saturation is presented as a fraction:

$$S_{wir} = \frac{V_{pore} - V_w}{V_{pore}} \tag{4.12}$$

where

$$\begin{aligned} S_{wir} &= \text{irreducible water saturation} && [-] \\ V_w &= \text{volume of produced water} && [cm^3] \end{aligned}$$

The volume of produced water is equal to the volume of oil injected into the core. Therefore, original oil in place (OOIP (cm^3) is found by knowing the volume of produced water (see Equation 4.13).

$$V_w = OOIP \tag{4.13}$$

4.6 Core Aging

Adsorption of carboxylic material onto the surface of rock defines a wetting property of carbonates (see section 2.1). Hopkins et al. (2016) used outcrop chalk material to scrutinize adsorption of carboxylic material onto a rock surface. They found that that adsorption occurs immediately as the oil contacts the rock changing wettability towards mixed-wet even without aging.

In spite of the fact mentioned above, it was decided to age the carbonate core plugs to achieve greater oil wetness of the rock. The core plugs were submerged into the crude oil inside of the metal core holder as soon as irreducible water saturation was established. The core holder was sealed and placed into the heating cabinet for core aging. The core plugs #B-2 and #B-3 were aged at 80°C for 14 days. The core plugs #B-1 and #B-8 were aged for 28 days.

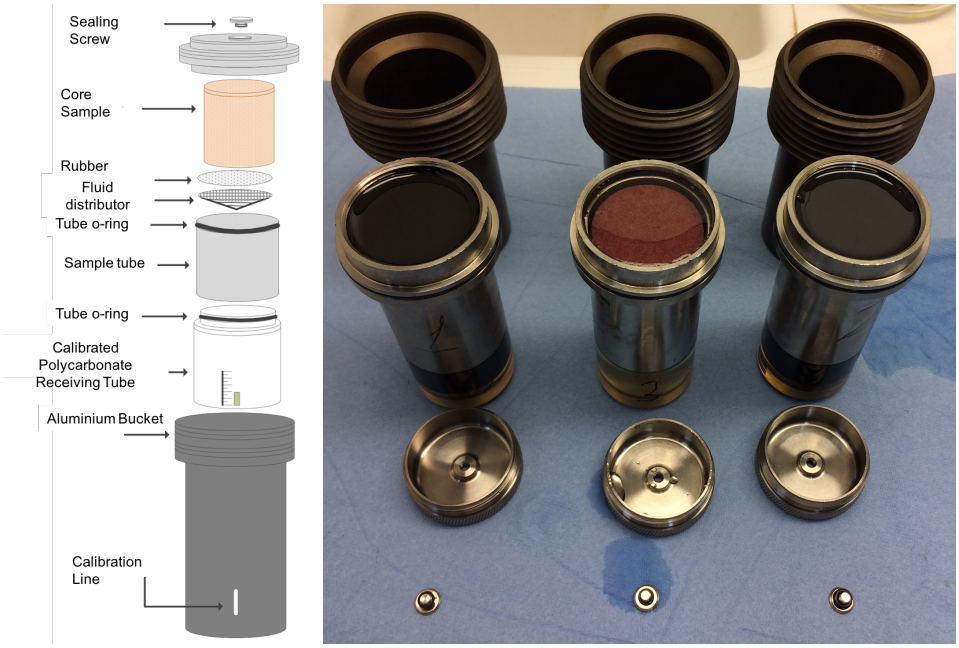

Figure 4.13: a) Schematic of centrifuge cup assembly. Diagram from Weatherford International (2013) b) drainage cup in the middle with a dummy core plug.

4.7 Spontaneous Imbibition Experiment

All glass made parts of the Amott cells were washed with soap and water and rinsed with distilled water. Afterward, the interior surface of the lids and tops of the cells were treated with acetone. This was done to prevent produced oil from sticking to the glass surface. The treated glass parts were placed into the heating cabinet at 60°C to dry overnight.

In total four core plugs were used for the experiments. The core plugs, namely #B-1, #B-2, #B-3 and #B-8, were chosen based on the results of core analysis (see section 5.2).

The o-rings of the Amott cells used for core #B-2 and #B-3 were treated with vacuum grease prior to installation. The o-rings were not greased for the cells used for core #B-1 and #B-8. The SI experiments were performed at 96°C in the heating cabinet. The imbibing brines were replaced in the cells as discussed in subsection 4.1.1.

4.7.1 Influence of Brine Salinity

Core #B-3. The lid of an Amott cell with all lines connected was placed into the heating cabinet at room temperature. A core stand was placed into the Amott cell lid. The core was removed from the aging core holder and rolled over the aluminium foil to remove excessive crude oil from the rock surface. The core plug was placed onto the core stand. The Amott cell was assembled and all lines were connected. The peristaltic pump was started. SFW was pumped into brine free Amott cell at 20 ml/min. When the water level reached the bottom edge of the core plug the rate was changed to 5 ml/min. Once the Amott cell was filled up, the heating cabinet was turned on.

Core #B-2. Since the heating cabinet had been already turned on, the Amott cell containing core plug #B-2 was assembled and filled up outside the eating cabinet at room temperature. SFW was pumped into brine free Amott cell at 20 ml/min. When the water level reached the bottom edge of the core plug the rate was changed to 5 ml/min. Once the Amott cell was filled up, the lines were disconnected and replaced with caps (first the top line and then the bottom line to avoid brine release from the cell). The cell was placed into the heating cabinet. The lines were connected to the cell (first the bottom line and then the top line to avoid brine release from the cell).

4.7.2 Influence of Brine Ion Composition

Core #B-1 and #B-8. Since the temperature in the heating cabinet had already been 96°C, Amott cells were assembled and filled up outside the heating cabinet at room temperature. The procedure was exactly the same as for core #B-2. The challenge was to avoid significant temperature decrease while placing the cells into the heating cabinet and connecting the lines as it could compromise the SI test on core #B-2 and core #B-3. Placement of the cells and connections was executed one step a time. If the temperature dropped close to 80°C while manipulations with the cell, the heating cabinet was closed to increase the temperature back to 96°C. The temperature inside the heating cabinet did not decrease below 80°C while the manipulations. It was assumed that the temperature of the brine inside of the cells did not change significantly because of large heat capacity of water.

Chapter 5

Results and Discussion

5.1 Properties of Liquids

5.1.1 Brine Composition

Synthetic waters were prepared using procedures described in subsection 4.2.1. Concentrations of ions were calculated using stoichiometry. A complete list of ions and their concentrations in SFW, SSW and 10dSSW is presented in Table 5.1. Total salinity of each brine is shown in Table 5.2 for comparison of liquids when considering reduced salinity experiments.

Table 5.1: Water ion compositions.

Ion [mg/l]	SFW	SSW	10dSSW	SSW2SO4	SSW4SO4
Na^+	57945	10592	1059.2	10036	8749
K^+	2890	396	39.6	396	396
Ca^{2+}	27118	409	40.9	409	409
Mg^{2+}	2741	1279	127.9	1279	1279
Sr^{2+}	4383	8	0.8	8	8
Cl^-	152241	19222	1922.2	16244	10289
SO_4^{2-}	0	2689	268.9	5378	10756
HCO_3^-	0	141	14.1	141	141
Ionic strength [mol/l]	5.133	0.700	0.070	0.700	0.700

Table 5.2: Brine salinity.

SFW [ppm]	SSW [ppm]	10dSSW [ppm]	SSW2SO4	SSW4SO4
247793	34822	3482	33890	32026

5.1.2 Interfacial Tension

The IFT was measured according to procedure in subsection 4.2.3. The measurements were performed at 25°C. The equilibrium of oil droplets in brines was reached after 2-3 hours. The results of the measurements are depicted in Figure 5.1 and summarized in Table 5.3. SFW has the highest IFT (17.46 mN/m) among all brines used in the SI test. SSW showed almost half the IFT of SFW (9.33 mN/m). Increase in IFT for 10dSSW (13.41 mN/m) in comparison with SSW is in line with what is reported by Mahani et al. (2015). SSW2SO4 and SSW4SO4 resulted in 10.43 and 9.53 mN/m respectively.

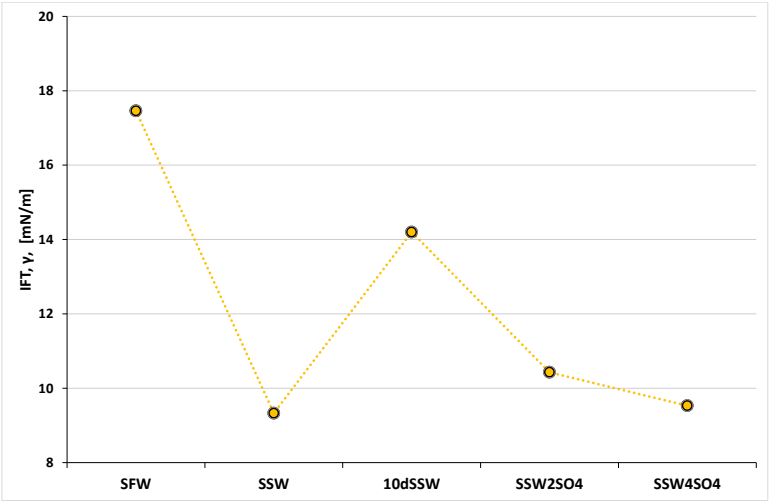

Figure 5.1: The comparison of IFT measurements for the brines used in the SI tests.

Table 5.3: Results of IFT measurements: Heidrun crude oil/brine.

Brine	SFW	SSW	10dSSW	SSW2SO4	SSW4SO4
IFT at 25°C [mN/m]	17.46	9.33	13.41	10.43	9.53

5.2 Core Analysis

5.2.1 Core Cutting

Carbonate core samples from Ainsa were cut according to procedure and requirements stated in section 4.3.1. Almost perfect edges of the cut surface were obtained for all the plugs. The core plugs were numbered from 1 to 8 with prefix B. Based on performed core analysis only four core plugs, namely #B-1, #B-2, #B-3 and #B-8, were chosen for the experiment and subsequently cleaned with methanol in Soxhlet extractor to remove dust from cutting and foreign particles. No color change of methanol was observed while cleaning. The core plugs were dried at 60°C for 5-6 days until the weight of the plugs became constant.

5.2.2 Core Dimensions

The length and diameter of the core plugs were measured as described in section 4.3.1. Cross-sectional area and total bulk volume of the cores were calculated using Equation 4.1 and Equation 4.2 respectively. The results are listed in Table 5.4.

Table 5.4: Core dimensions.

Core	L [cm]	d [cm]	A [cm^2]	V_{bulk} [cm^3]
#B-1	4.62	3.80	11.33	52.33
#B-2	4.59	3.81	11.43	52.43
#B-3	4.61	3.82	11.44	52.68
#B-4	4.61	3.82	11.45	52.80
#B-5	4.60	3.71	10.81	49.73
#B-6	4.42	3.80	11.36	50.15
#B-7	4.59	3.81	11.41	52.43
#B-8	4.56	3.81	11.41	52.03

5.2.3 Porosity and Pore Volumes

The results of porosity and pore volumes measurements using helium porosimeter are presented in Table 5.5. All calculations were performed as shown in subsection 4.3.2. The core #B-1, #B-2, #B-3 and #B-8 have similar pore volumes, V_{pore}, and porosity, ϕ_e. These core plugs were selected for the experiments and saturated with water based on porosity results and permeability measurements (see subsection 5.2.5). The result of porosity and permeability measurements using liquid saturation method are shown in Table 5.6.

Table 5.5: Data of pore volume and effective porosity measurements using helium porosimeter.

Core	V_{cup} [cm^3]	$V_{cup+core}$ [cm^3]	V_{grain} [cm^3]	V_{pore} [cm^3]	ϕ_e
#B-1	68.00	26.55	41.45	10.88	20.80
#B-2	68.00	26.20	41.80	10.63	20.27
#B-3	68.00	26.10	41.90	10.78	20.46
#B-4	68.00	24.50	43.50	9.30	17.61
#B-5	69.00	25.90	43.10	6.63	13.33
#B-6	69.00	28.10	40.90	9.25	18.44
#B-7	69.00	25.15	43.85	8.58	16.37
#B-8	69.00	27.00	42.00	10.03	19.27

Table 5.6: Data of pore volume and effective porosity measurements using liquid saturation method

Core	W_{dry} [g]	W_{wet} [g]	V_{pore} [cm^3]	ϕ_e [%]
#B-1	111.889	123.878	10.232	19.55
#B-2	112.779	124.195	9.743	18.58
#B-3	112.993	124.695	9.987	18.96
#B-8	110.918	122.564	9.939	18.96

5.2.4 Grain Density

Equation 4.7 were used to calculate grain density of the core plugs. Result are shown in Table 5.7. The grain density varied among the core plugs, suggesting that the matrix consists of several minerals and their fraction might be slightly different in each core plug.

Table 5.7: Results of grain density calculations.

Core #	B-1	B-2	B-3	B-4	B-5	B-6	B-7	B-8
ρ_{grain} [g/cm^3]	2.70	2.70	2.70	2.71	2.64	2.64	2.65	2.64

5.2.5 Permeability

The air permeability measurements were performed according to subsection 4.3.4. The data obtained from the permeability tests on all core plugs is presented in Appendix A. The air permeabilities at different mean pressures were calculated using Equation 4.8 and plotted versus the reverse of the mean pressures. Obtained graphs were extrapolated to infinite pressure in Figure 5.2 and Figure 5.3. Linear equations representing the extrapolated graphs correspond to Equation 4.9. Liquid permeability values were found from the linear equations. Klinkenberg correction factor was found from the slope of the graph according to Equation 5.1. Results are presented in Table 5.8.

$$b = \frac{m}{k_L} \tag{5.1}$$

where

k_L liquid permeability	$[mD]$
$b =$ correction factor	$[-]$
$m =$ slope of the graph	$[-]$

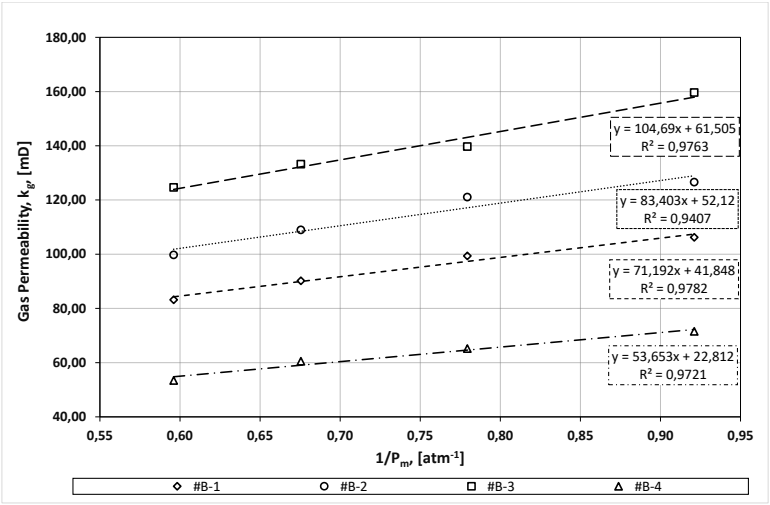

Figure 5.2: The gas permeability versus reverse of the mean pressure for core plugs #B-1 to #B-4.

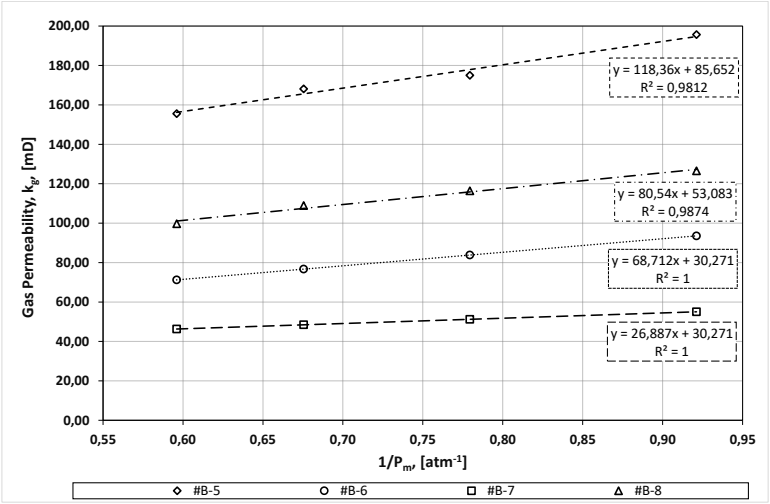

Figure 5.3: The gas permeability versus reverse of the mean pressure for core plugs #B-5 to #B-8.

Table 5.8: Results of Klinkenberg corrected permeability

Core #	B-1	B-2	B-3	B-4	B-5	B-6	B-7	B-8
k_L [mD]	41	52	62	23	86	30	30	53
b	71.19	83.40	104.7	53.65	118.36	68.71	26.89	80.5

5.2.6 Mineral Composition

Mineral composition of the Ainsa carbonate was studies using X-Ray Diffraction (XRD) and Energy-dispersive X-ray spectroscopy (EDS) techniques.

XRD was performed on the powder of one sample of Ainsa carbonate by laboratory engineer Laurentius Tijhuis at the Department of Geoscience and Petroleum, NTNU. The results of XRD substantiated the assumption that rock matrix consist of several minerals. Table 5.9 shows that at least three minerals are present in the crushed rock material: calcite, quartz and K-feldspar. The XRD spectra is plotted in Figure A.1.

Table 5.9: Results of XRD test.

Calcite [%]	Quartz [%]	K-feldspar [%]
86.10	13.01	0.89

EDS was performed on four thin sections of Ainsa carbonate at the Norwegian Laboratory for Minerals and Material Characterisation (MiMaC). The thin sections were prepared at the Thin Sections laboratory at the Department of Geoscience and Petroleum, NTNU by

Håkon Fjærli. The thin sections were numbered from 1 to 4 with prefix C. The results of EDS are presented in Table 5.10. It was found that fluorite and apatite are also present in the rock matrix in a very low amounts. Figure 5.4 depicts EDS/SEM image of the thin section #C-4. No anhydrite was found from XRD and EDS studies. Hence, Ainsa carbonate was classified as anhydrite free limestone (Gary, 2009).

Table 5.10: Results of SEM/EDS. Table shows weight % of each mineral.

Thin section #	C-1	C-2	C-3	C-4
Carbonate	80.02	83.22	84.35	86.58
Quartz	17.69	14.67	13.96	11.96
K-feldspar	1.58	1.44	1.09	0.74
Fluorite	0.57	0.59	0.47	0.58
Apatite	0.15	0.08	0.13	0.14
Unclassified	0.00	0.00	0.00	0.00

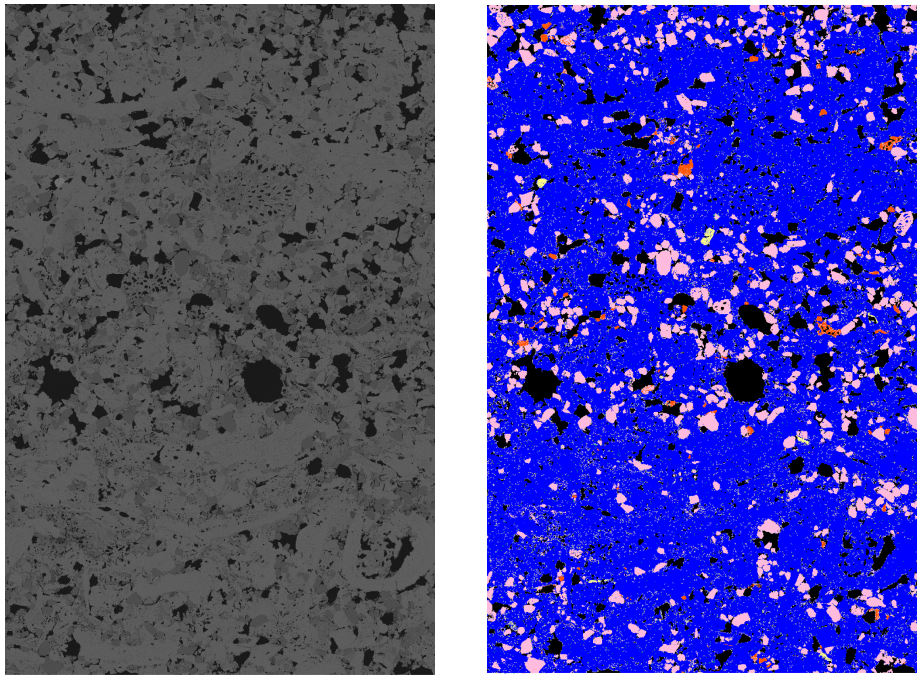

(a) **(b)**

Figure 5.4: a) Gray Scale SEM image of thin section #C-4; b) EDS image of thin section #C-4: here carbonate - blue, quartz -pink, K-feldspar - red, fluorite - green, apatire - yellow.

5.3 Zeta Potential

Zeta potential measurements were performed as described in section 4.4. The results are depicted in Figure 5.5 and summarized in Table 5.11. Zeta potential of SFW (21.5mV) is not directly comparable with other brines because of a significant difference in pH, however zeta potential is expected to increase with higher pH (Mahani et al., 2015). Therefore, SSW shows less positive value (7.9mV) in comparison with SFW. The change in zeta potential can be explained by EDL expansion due to salinity reduction (Mahani et al., 2017), and adsorption of sulfate to the rock surface (Zhang and Austad, 2006).

Spiking SSW with twice sulfate (SSW2SO4) changed the zeta potential towards an even more negative value (-1.3mV). When the concentration of sulfate was increased to four times (SSW4SO2) of the concentration in SSW, the zeta potential decreased even more (-6.9mV). 10dSSW showed the most negative zeta potential (-8.1), indicating that this water causes the strongest repulsion between oil-water and rock-water interfaces. Zeta potential for oil emulsion in brines was not measured. Crude oil-water interface is believed to have a negative charge at the pH range reported for the considered brines (Mahani et al., 2015; Alotaibi and Nasr-El-Din, 2011)

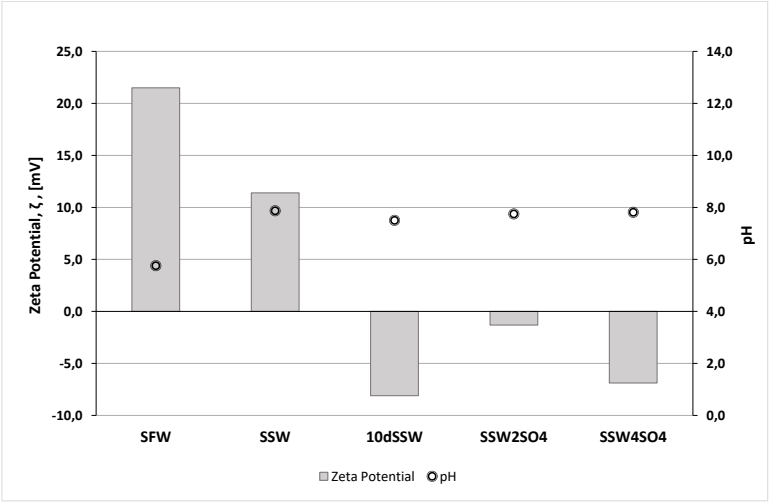

Figure 5.5: Zeta potential and pH of the brines at 25°C.

Table 5.11: Results of zeta potential measurements and pH of the brines at 25°C

Brine	SFW	SSW	10dSSW	SSW2SO4	SSW4SO4
Zeta potential 25°C [mV]	21.5	11.4	-8.1	-1.3	-6.9
pH at 25 °C	5.8	7.9	7.5	7.8	7.8

5.4 Saturation of Core Plugs

Saturation of the core plugs with SFW was executed as described in subsection 4.5.1. The core plugs selected for the experiment were saturated with filtered and degassed crude oil using a Beckman centrifuge at 5000 rev/min following the procedure presented in subsection 4.5.2. Produced water was collected in burettes in order to find OOIP and irreducible water saturation, S_{wir}.

Equation 4.13 and Equation 4.12 was used to calculate OOIP and S_{wir}, respectively. Results of the calculations are shown in Table 5.12. Centrifuging at more than 5000 rev/min to decrease S_{wir} was not attempted as there was a risk to damage the core plugs.

Table 5.12: Results of OOIP measurements.

Core #	B-1	B-2	B-3	B-8
OOIP [cm^3]	6.8	5.8	5.4	6.7
S_{wir} [-]	0.34	0.40	0.46	0.35

5.5 Spontaneous Imbibition Experiment

5.5.1 Influence of Brine Salinity

Initially, the core plugs #B-2 and #B-3 were submerged into SFW as described in subsection 4.7.1. Recovery readings were taken on a daily basis, except during the first four hours of the experiment when the oil production was recorded every 30 minutes. The oil recovery during this time was 8.6% and 3.7% from core #B-2 and #B-3 respectively, which can be related to thermal expansion of rock matrix and fluids. The difference in the production can be explained by the difference in pore structure, however no micro CT images are available for the core plugs to support this assumption.

The oil recovery as a function of time is presented in Figure 5.6. The recovery plateau under SFW was reached for both core plugs on day 19 of spontaneous imbibition test. The oil recovery from core #B-2 was about 35%, while from core #B-3 it was 27%. After 8 and 10 days of plateau recovery for core #B-2 and core #B-3 respectively, the imbibing brine was replaced with SSW. Positive response to SSW for both core plugs was observed a day after brine replacement. The oil recovery soared, and over next 27 days made up about 53% for core #B-2 and 37% for core #B-3. The LSR under SSW was approximately 18% and 10% for core #B-2 and core #B-3 respectively. The core plugs were left in SSW for more than 10 days during the recovery plateau. Afterwards SSW was replaced with 10dSSW. No LSR was observed for core #B-2 over 30 days of being exposed to 10dSSW. Incremental oil recovery for core #B-3 was less than 1%. The LSR from core #B-3 a was observed after 12 days of imbibition with 10dSSW and made up about 1%.

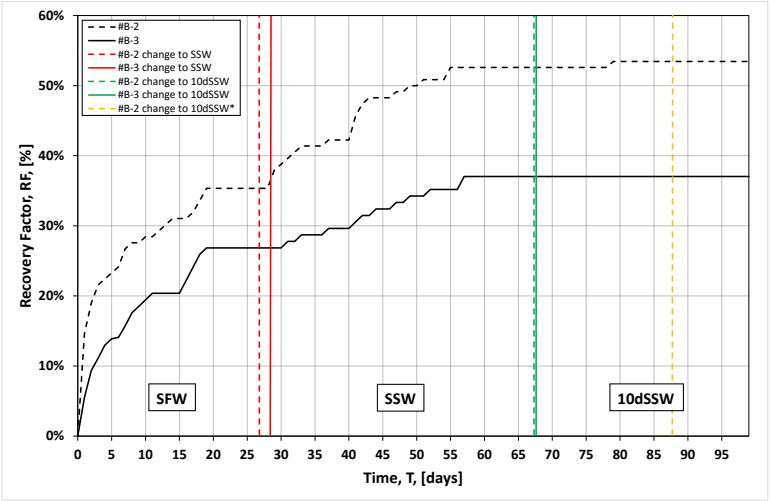

Figure 5.6: The oil recovery from core#B-2 and #B-3. Readings were taken at ambient conditions. SFW, SSW and 10dSSW were used as imbibing brines.

On day 88 the Amott cell containing core #B-2 was removed from the heating cabinet and 10dSSW was refreshed as described in subsection 4.7.1. The goal was to scrutinize whether extra core handling will result in incremental oil recovery (see section 2.3). No additional oil was produced in this specific case.

During the SI test with SFW it was noticed that oil is not homogeneously produced from all the open faces of the core plugs. It is depicted in Figure 5.7a that the oil exit the plug mainly from the top of the lateral face and from the top face, but almost no oil droplets exit the plug on the bottom of the lateral face. This indicates that gravity forces were present in the imbibition process along with capillary forces. Figure 5.7b shows that when imbibing brine was changed to SSW, the oil was produced from the top face of the core plug only, suggesting that gravity forces became more important in the imbibition process. It is worth to note that there were numerous oil droplets on the lateral face of the core which did not detach throughout the plateau period under SFW. They were not removed from the core surface during the brine replacement process as well, highlighting the stability of the crude oil/brine/rock system during brine replacement by the developed method (see subsection 4.1.1). Eventually droplets on the lateral face detached a day after being exposed to SSW, while the oil resumed to exit from the top face of the core plug under gravity influenced imbibition.

In the literature, switch to gravity dominated imbibition is explained by reduction in IFT of imbibing brine, which decreases the ratio of capillary forces to gravity forces (also known as inverse of Bond number) (Schechter et al., 1994; Al-Lawati and Saleh, 1996; Høgnesen et al., 2006). However, IFT of SSW used in this thesis does not correlate with IFT reported in mentioned papers. It is assumed that initially oil is recovered homogeneously because of high imbibition rate. Later, when the imbibition rate is decreased, liquids inside of the

core plug have enough time to segregate due to gravity and production is observed mainly from the top face. Spontaneous imbibition under gravity dominated flow is known to have slower imbibition rate, but higher oil recovery in comparison with capillary dominated flow (Schechter et al., 1994). Thus, the change in the recovery driving forces might have contributed to increased oil recovery when SFW was replaced by SSW.

If Young equation is considered (see Appendix C), one can see that a decrease in IFT changes the contact angle to a less oil wetting state. Hence, almost double reduction in IFT indicates that its contribution to contact angle change and consequently incremental oil recovery under SSW cannot be excluded. Zeta potential measurements suggest smaller attractive forces between the oil and rock surface under SSW compared to SFW because of EDL expansion, which causes alteration in wettability and change of contact angle to a more water wet state as shown in Figure 2.28 (Mahani et al., 2017). Moreover, unlike SFW, SSW contains SO_4^{2-} in its composition, which is known to be a wettability alteration catalyst (Zhang et al., 2007). Therefore, there is a combination of many factors contributing into a dramatic increase in recovery when imbibition brine was changed from SFW to SSW. However, it is not possible to estimate the significance of the particular factors in enhanced oil recovery from these experiments. Overall, it can be said that SSW is an effective EOR fluid for the crude oil/brine/rock system used in the SI test.

Overall 10dSSW was not able to improve oil recovery from both core plugs. The core #B-2 imbibing with 10dSSW is presented in Figure 5.7c.

Zeta potential measurements of limestone suspension in 10dSSW showed negative values suggesting that there is EDL expansion and contact angle changes towards a less oil wet state (Mahani et al., 2017). On the other hand, IFT for 10dSSW is higher than that for SSW by 4 units, 13.41 and 9.33 mN/m respectively. If only IFT is considered, it is deduced from the Young equation that a contact angle changes towards a more oil wet state. Therefore, one can argue that EDL expansion and IFT increase have opposite impact on wettablity alteration. On the other hand, maximum oil recovery is expected at close to neutral wet conditions (Jadhunandan and Morrow, 1995; Anderson, 1987). One might argue that SSW had already changed wettability of rock to neutral wet before the core plugs were introduced to 10dSSW. Hence, altering wettability to more water-wet conditions by 10dSSW did not lead to additional LSR.

Several authors showed positive response to reduced salinity water in carbonates when anhydrite was present in rock matrix (Yousef et al., 2011; Austad et al., 2015, 2012). Anhydrite dissolves upon dilution of imbibing brine, which causes in situ formation of SO_4^{2-} (Austad et al., 2012) and at the same time smaller concentration of NaCl in diluted water provides better access of PDIs to rock surface (Fathi et al., 2012), which in combination causes wettablity alteration and LSR. The results of XRD and EDS tests showed that there is no anhydrite in Ainsa limestone. Fathi et al. (2012) and Austad et al. (2012) showed no incremental oil recovery from anhydrite free carbonates. Shariatpanahi et al. (2011) reported LSR from anhydrite free dolomite when SSW water was diluted 10 times. However, AN of the oil used in their experiment is significantly lower than AN of our Heidrun oil (0.52 and 2.9 mg KOH/g respectively), which suggests smaller content of carboxylic material governing wettability in carbonates (Zhang and Austad, 2005). It is assumed that

the small concentration of PDIs in 10dSSW and the lack of anhydrite cannot be compensated by EDL expansion because of high content of carboxylic material in Heidrun crude oil. However, more research has to be done to investigate this. It is suggested to scrutinize the impact of AN on response of anhydrite free carboante rock to diluted versions of SSW in tertiary mode.

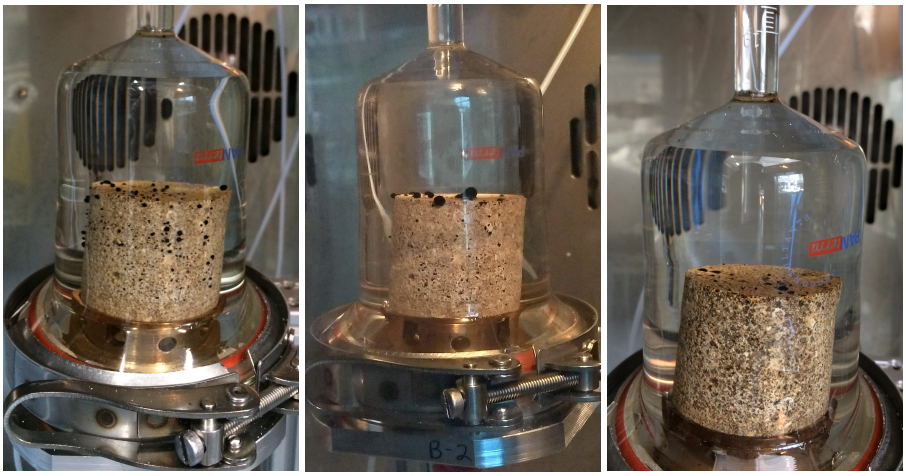

(a) SFW **(b)** SSW **(c)** 10dSSW

Figure 5.7: Distribution of oil droplets on the surface of core #B-2 during spontaneous imbibition with different brines.

5.5.2 Influence of Brine Ion Composition

Initially, the core plugs #B-1 and #B-8 were submerged into SSW at room temperature as described in subsection 4.7.2. Recovery reading were taken on a daily basis, except during the first four hours of the experiment when the oil production was recorded every 30 minutes. Negligible amount of oil was produced from core plug #B-1 during this time, while oil recovery from core plug #B-8 made up about 6%. However, oil production readings showed similar recoveries on the next day: about 15% and 18% from core plug #B-1 and core plug #B-8 respectively. The oil recovery as a function of time is presented in Figure 5.8.

The recovery plateau under SSW was reached for both core plugs on day 27 of spontaneous imbibition test. The oil recovery from core #B-1 was about 37%, while from core #B-8 it was 38%. The oil recovery from core #B-1 and #B-8 under SSW is very similar to what was obtained for #B-2 and #B-3 under SFW. However, it has to be taken into account that core plug #B-1 and #B-8 were aged for 28 days, while core plug #B-2 and #B-3 for 14 days. Therefore wetting property of core plug #B-1 and #B-8 assumed to be more oil wet. After 9 and 10 days of plateau recovery for core #B-1 and core #B-8 respectively, the imbibing brine was replaced with SSW2SO4. Positive response to SSW2SO4 for core plugs

was observed after 2-3 days of imbibition. Additional oil recovery for core #B-1 and core #B-8 was 3% and 1.5% respectively over the time of imbibition with SSW2SO4. After 5 days under recovery plateau experiment was stopped for core #B-1. Imbibing brine was changed for core #B-8 after 7 days under plateau. SSW2O4 was replaced with SSW4SO4, which recovered additional 3% of oil over 15 days. Overall LSR under imbibition with SSW2SO4 and SSW4SO4 combined made up about 4.5% for core plug #B-8.

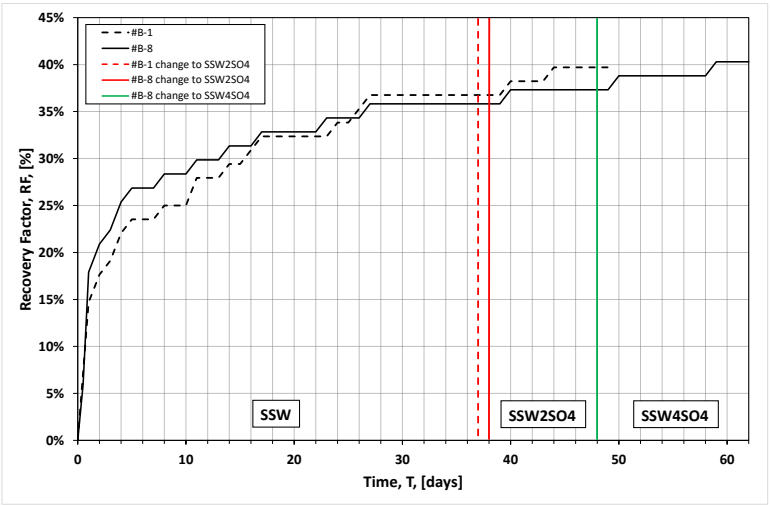

Figure 5.8: The oil recovery from core#B-1 and #B-8. Readings were taken at ambient conditions. SSW, SSW2SO4 and SSW4SO4 were used as imbibing brines.

Ravari (2011) found that outcrop limestone material from two different locations used in his studies was not reactive to PDIs based on chromatographic separation test and zeta potential measurements. He assumed that this is because outcrop material has been exposed to aerobic conditions, however no clear reason was deduced. Opposite can be said about reactivity of the Ainsa limestone with PDIs, as zeta potential changed from positive to negative when concentration of SO_4^{2-} was increased twice in SSW. Zeta potential decreased to even more negative values when concentration of SO_4^{2-} was increased four times in SSW. Hence, it can be concluded that Ainsa limestone is reactive to PDIs, and that SO_4^{2-} adsorbs onto the rock surface and changes the surface charge.

All in all, SSW spiked with SO_4^{2-} increased oil recovery from Ainsa limestone, but the results are not comparable to the significantly higher incremental oil recoveries reported for chalk (Romanuka et al., 2012; Zhang et al., 2006). This can be explained by lower reactivity of limestone to PDIs in comparison with chalk (Strand et al., 2008). On the other hand, Fernø et al. (2011) argues that the sulfate effect is sensitive to the oil/brine/rock system, as they observed less incremental oil recovery from Stevns Klint chalk than it was reported in previous papers (e.g. Zhang et al. (2006)). Moreover, from their study, Fernø et al. (2011) concluded that the effect of sulfate on wettability alteration becomes less significant as the rock becomes more water-wet. It is found from SI test on core #B-2 and

#B-3 that SSW significantly changes wettablity of Ainsa limestone towards more water-wet. This might be a reason of the low effect of SO_4^{2-} on wettability alteration in #B-1 and #B-8 as the wetting state had already been significantly changed towards more water-wet by SSW before the core plugs were exposed to SSW2SO4 and SSW4SO4.

5.5.3 Experimental Setup

In general, the assembled experimental setup behaved as expected when it comes to brine replacement. Imbibing brines were successfully changed without any observed issues. The ohmmeter readings were used to qualitatively substantiate the replacement of the brines. However, air dissolved in the brines became a major problem for this setup. Although all the brines were degassed as described in subsection 4.2.1, air bubbles were observed in the Amott cells at 96°C. It is important to note that degassed brines were checked for air content by heating up to 96°C in an Anton Paar density meter as shown in Figure 5.9 prior to pumping them into the cells.

The air bubbles attached to core surface and all hydrophobic surfaces in the Amott cells, e.g. oil droplets stuck on the glass surface of the cell and on the greased o-ring of the Amott cell. To most extent the air issue was observed for core #B-1 and #B-8, as the o-rings were not greased in this case; therefore all the air adsorbed on the surface of the core plugs and core stands. For core #B-2 and #B-3 less air droplets were observed on the core surface as the the air mainly attached to greased o-rings of the Amott cells. The air issue was not identified while testing the setup. The reason is believed to be the use of Exxsol D-60 instead of crude oil while testing the setup. Furthermore, the grease applied to the o-rings in this case might have led the air issue being unnoticed.

Another issue was salt precipitation in ”vapour out” lines because of brine vaporisation. Precipitated salt blocked tee valves from time to time on the bottom of the Amott cells (top tee valves had no issues). In order to unclog the valves, a brine was continuously pumped into the ”vapour out” lines. Pressure build up brought brines in contact with accumulated salt, and dissolved it. It is important to highlight that tee valve were turned in the direction of ”vapour line” during this manipulations, hence there was no pressure build up in the Amott cells. The issue was observed only for the Amott cells which were used for core #B-2 and #B-3. It is believed that the issue was initially caused by highly saline SFW and later abraded valve (because of exposure to SFW) became a spot for salt accumulation even when SSW and 10dSSW were used as imbibing brines. On day 65 of the SI experiment, the tee valve on the bottom of the Amott cell containing core #B-2 failed. It was not possible to unclog the plug by pressure build up. Therefore, the tee valve was disconnected from the Amott cell. The valve was cleaned from salt by flushing it with distilled water. Meanwhile the Amott cell outlet was closed with a cap. Once the valve was cleaned it was installed back. The problem occurred while core #B-2 was under plateau recovery with SSW as imbibing brine. There was no incremental oil recovery over the next 3 days after the issue. Therefore it is believed that removing the valve for cleaning did not compromise the experiment. The salt issue was not identified while testing the setup as it appeared only during the long-term experiment.

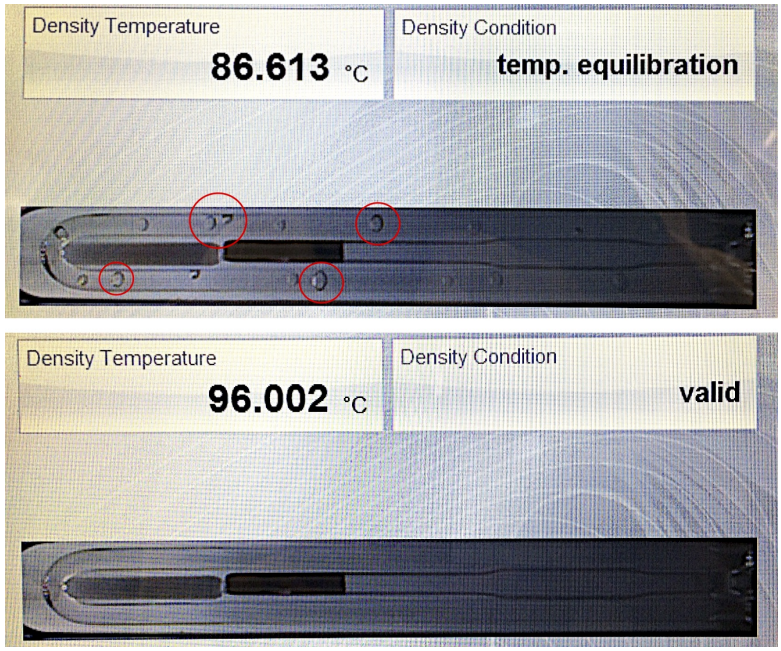

Figure 5.9: Air content check at high temperature using Anton Paar density meter. Top image: air starts to expand (red circles) in non degassed brine at 86°C; Bottom image: no signs of air at 96°C.

Chapter 6

Conclusions

One of the goals of the thesis was to investigate the effect of Low Salinity EOR on wettability alteration in carbonate outcrop core plugs from the Ainsa Basin in the Spanish Pyrenees, which are selected to represent reservoir rock of carbonate field in Brazil operated by Equinor. Two sets (two core plugs for each) of SI tests were performed at 96°C. One set examined influence of salinity (SFW, SSW, 10dSSW), while another set the influence of ionic composition (SSW, SSW2SO4, SSW4SO4) on wettability alteration. The SI tests were supported by zeta potential measurements, interfacial tension and mineralogy studies. Mineralogy of the rock was examined by means of XRD and SEM/EDS. Zeta potential was measured on aqueous solutions of carbonate particles. Heidrun crude oil with AN = 2.9 mg KOH/g was used in the experiments. The main conclusions from the conducted experiments are:

- XRD results showed that Ainsa carbonate consists of several minerals: calcite (86.10%), quartz (13.01%) and K-feldspar (0.89%). SEM/EDS substantiated this data and found additional minerals: fluorite and apatite (both in a very small amount). No anhydrite was found in Ainsa carbonate. Based on mineralogy study Ainsa carbonate was classified as limestone.

- Zeta potential measurements (at 25°C) showed that outcrop material from Ainsa is reactive with SO_4^{2-}. Zeta potential decreased from 11.4mV for SSW to -1.3mV for SSW2SO4 and -6.9mV for SSW4SO4. 10dSSW showed the most negative zeta potential (-8.1mV), while SFW the most positive (21.5mV).

- IFT decreased in the order: SFW (17.46mN/m) $>$ 10dSSW (13.41mN/m) $>$ SSW (9.33mN/m). IFT of SSW2SO4 and SSW4SO4 was comparable with SSW.

- SSW is the most effective Low Salinity EOR fluid for the crude oil-brine-rock system used in the SI tests. Incremental oil recovery upon replacement of SFW with SSW made up about 18% and 10% for core plug #B-2 and #B-3 respectively. It

is believed that many factors contributed to significant LSR: EDL expansion, PDIs, decrease in IFT.

- No additional oil recovery was observed when the core plugs #B-2 and #B-3 were exposed to 10dSSW. It is shown that there is no incremental oil recovery upon dilution of SSW when the rock matrix is anhydrite free.
- SSW as the first imbibing brine for core plug #B-1 and #B-8 produce 37% and 38% of OOIP respectively.
- SSW2SO4 and SSW4SO4 slightly improved oil recovery from core plug #B-1 and #B-8. SSW2SO4 recovered additional 3% from core plug #B-1, while only 1.5% for core plug#B-8 respectively. When SSW2SO4 was replaced by SSW4SO4 for core plug #B-8, incremental oil recovery made up about 3%.

Another goal of the thesis was to develop an experimental setup, which allows replacing one imbibing brine with another without interruption of the SI test. The following can be concluded:

- The assembled setup behaved as it was designed when it comes to brine replacement. The brine replacement in each set of experiments was performed with no issues and substantiated qualitatively by means of resistivity using an ohmmeter.
- Although all brines were degassed and air content was checked at 96°C prior to brine replacement, air dissolved in the brines became the main problem of the setup.
- Air attached to all hydrophobic surface, including the surface of the core plugs. The problem was more remarkable for core plug #B-1 and #B-8 than for #B-2 and #B-3.
- Salt precipitation in the lines because of brine vaporisation affected the performance of tee valves on the bottom of the Amott cells. This resulted in the failure of the tee valve on the Amott cell containing core plug #B-2. No issues were observed for the tee valves on top of the cells.

For further work, it is recommended to pressurize the new experimental setup to prevent brine vaporization in the lines and observed air issue. It is also suggested to install remotely operated tee valves instead of manually operated on the top and bottom of the Amott cells, which will eliminate the necessity to open the heating cabinet.

It is suggested to investigate the impact of AN on the response of anhydrite free carbonate rock to diluted versions of SSW. It is assumed that reduced concentration of PDIs in diluted SSW cannot be compensated by EDL expansion when oils with high AN are used.

Bibliography

Al-Khafaji, A., Wen, D., 2019. Quantification of wettability characteristics for carbonates using different salinities. Journal of Petroleum Science and Engineering 173, 501 – 511, https://doi.org/10.1016/j.petrol.2018.10.044.

Al-Lawati, S., Saleh, S., 1996. Oil recovery in fractured oil reservoirs by low ift imbibition process. SPE Annual Technical Conference and Exhibition, 6-9 October, Denver, Colorado, https://doi.org/10.2118/36688-MS.

Alotaibi, M. B., Nasr-El-Din, H. A., 2011. Electrokinetics of limestone particles and crude-oil droplets in saline solutions. SPE Reservoir Evaluation & Engineering 14 (05), 604–611, https://doi.org/10.2118/151577-PA.

Anderson, W., 1987. Wettability literature survey- part 4: Effects of wettability on capillary pressure. Journal of petroleum Technology 39 (10), 1283–1300, https://doi.org/10.2118/15271-PA.

Anderson, W. G., 1986. Wettability literature survey - part 2: Wettability measurement. Journal of Petroluem Technology 38 (11), 1246 – 1262, https://doi.org/10.2118/13933-PA.

Austad, T., Shariatpanahi, S. F., Strand, S., Aksulu, H., Puntervold, T., 2015. Low salinity eor effects in limestone reservoir cores containing anhydrite: A discussion of the chemical mechanism. Energy & Fuels 29 (11), 6903–6911, https://doi.org/10.1021/acs.energyfuels.5b01099.

Austad, T., Shariatpanahi, S. F., Strand, S., Black, C. J. J., Webb, K. J., 2012. Conditions for a low-salinity enhanced oil recovery (EOR) effect in carbonate oil reservoirs. Energy & Fuels 26 (1), 569–575, https://doi.org/10.1021/ef201435g.

Azizov, I., 2018. Master's specialization project - Effect of water quality on wettability alteration in carbonates. Norwegian University of Science and Technology.

Bartels, W.-B., Mahani, H., Berg, S., Hassanizadeh, S., 2019. Literature review of low

salinity waterflooding from a length and time scale perspective. Fuel 236, 338 – 353, https://doi.org/10.1016/j.fuel.2018.09.018.

Buchner, R., Hefter, G. T., May, P. M., 1999. Dielectric relaxation of aqueous nacl solutions. The Journal of Physical Chemistry A 103 (1), 1–9, https://doi.org/10.1021/jp982977k.

Butt, H., Graf, K., Kappl, M., 2003. Physics and Chemistry of Interfaces, 1st Edition. Wiley-VCH.

Chilingar, G. V., Yen, T. F., 1983. Some notes on wettability and relative permeabilities of carbonate reservoir rocks, II. Energy Sources 7 (1).

Fathi, S. J., Austad, T., Strand, S., 2012. Water-Based Enhanced Oil recovery EOR by "Smart Water" in Carbonate Reserovirs. Society of Petroleum Engineers, SPE EOR Conference at Oil and Gas West Asia, 16-18 April, Muscat, Oman, https://doi.org/10.2118/154570-MS.

Gary, N., 2009. Sedimentology and Stratigraphy, 2nd Edition. Wiley-Blackwell, Chichester, UK ; Hoboken, NJ.

Han, K. N., 2002. Fundamentals of Aqueous Metallurgy. Society for Mining, Metallurgy, and Exploration (SME), https://app.knovel.com/hotlink/toc/id:kpFAM00011/fundamentals-aqueous/fundamentals-aqueous.

Hiorth, A., Cathles, L., Madland, M., 2010. The impact of pore water chemistry on carbonate surface charge and oil wettability. Transport in Porous Media 85 (1), 1–21, https://doi.org/10.1007/s11242-010-9543-6.

Hirasaki, G., 1991. Wettability: Fundamentals and surface forces. SPE Formation Evaluation 6 (2), 217–226, https://doi.org/10.2118/17367-PA.

Hirasaki, G., Zhang, D., 2004. Surface chemistry of oil recovery from fractured, oil-wet carbonate formations. SPE Journal 9 (2), 151–162, https://doi.org/10.2118/88365-PA.

Hopkins, P. A., Walrond, K., Strand, S., Puntervold, T., Austad, T., Wakwaya, A., 2016. Adsorption of acidic crude oil components onto outcrop chalk at different wetting conditions during both dynamic adsorption and aging processes. Energy & Fuels 30 (9), 7229–7235, https://doi.org/10.1021/acs.energyfuels.6b01583.

Jadhunandan, P., Morrow, N., 1995. Effect of wettability on waterflood recovery for crude-oil/brine/rock systems. SPE Reservoir Engineering 10 (1), 40–46, https://doi.org/10.2118/22597-PA.

Klinkenberg, L., 1941. The permeability of porous media to liquids and gases. American Petroleum Institute, Drilling and Production Practice, 1 January, New York, New York.

Korsnes, R., Strand, S., Hoff, Ø., Pedersen, T., Austad, T., 2006. Does the chemical interaction between seawater and chalk affect the mechanical properties of chalk? In: Cottheim, A., Charlies., R., Thimus, J., Tshibangu, J. (Eds.), EUROCK 2006: Multiphysics Coupling and Long Term Behaviour in Rock Mechanics. Taylor & Francis, pp. 427–434.

Legens, C., Toulhoat, H., Cuiec, L., Villieras, F., Palermo, T., 1999. Wettability change related to adsorption of organic acids on calcite: Experimental and ab initio computational studies. SPE Journal 4 (4), 328 – 333, https://doi.org/10.2118/57721-PA.

Mahani, H., Keya, A. L., Berg, S., Bartels, W.-B., Nasralla, R., Rossen, W. R., 2015. Insights into the mechanism of wettability alteration by low-salinity flooding (lsf) in carbonates. Energy & Fuels 29 (3), 1352–1367, https://doi.org/10.1021/ef5023847.

Mahani, H., Keya, A. L., Berg, S., Nasralla, R., 2017. Electrokinetics of carbonate/brine interface in low-salinity waterflooding: Effect of brine salinity, composition, rock type, and ph on ζ-potential and a surface-complexation model. SPE Journal 22 (1), 53–68, https://doi.org/10.2118/181745-PA.

Malvern Instruments Ltd, 2013. ZETASIZER NANO SERIES USER MANUAL. https://www.malvernpanalytical.com/en/learn/knowledge-center/user-manuals/MAN0485EN.html, accessed 30.05.2019.

Mjos, J. E. S., Strand, S., Puntervold, T., Gaybaliyev, H., 2018. Effect of initial wetting on smart water potential in carbonates. SPE EOR Conference at Oil and Gas West Asia, 26-28 March, Muscat, Oman, https://doi.org/10.2118/190414-MS.

Morrow, N. R., 1990. Wettability and its effect on oil recovery. Journal of Petroleum Techonlogy 42 (12), pp. 1476–1484, https://doi.org/10.2118/21621-PA.

Nasralla, R. A., Mahani, H., van der Linde, H. A., Marcelis, F. H., Masalmeh, S. K., Sergienko, E., Brussee, N. J., Pieterse, S. G., Basu, S., 2018. Low salinity waterflooding for a carbonate reservoir: Experimental evaluation and numerical interpretation. SPE Improved Oil Recovery Symposium, 14-18 April, Tulsa, Oklahoma, USA 164, 640–654, https://doi.org/10.1016/j.petrol.2018.01.028.

PanTerra Geoconsultants, 2018. Personal communication.

Petrovich, R., Hamouda, A., 1998. Dolomitization of Ekofisk reservoir chalk by injected seawater, in: Paper Presented at Ninth International Symposium on Water-Rock Interactions, Taupo, New Zealand, March 30 - April 3. Oilfield Chemistry Symposium of the Society of Petroleum Engineers of AIME, May 24-25.

Pollen, E. N., Berg, C. F., 2018. Experimental investigation of osmosis as a mechanism for low-salinity EOR. Abu Dhabi International Petroleum Exhibition & Conference, 12-15 November, Abu Dhabi, UAE, https://doi.org/10.2118/192753-MS.

Ravari, R. R., 2011. Water-based EOR in limestone by smart water. Ph.D. thesis, University of Stavanger.

Romanuka, J., Hofman, J., Ligthelm, D. J., Suijkerbuijk, B., Marcelis, F., Oedai, S., Brussee, N., van der Linde, H., Aksulu, H., Austad, T., 2012. Low salinity EOR in carbonates. SPE Improved Oil Recovery Symposium, 14-18 April, Tulsa, Oklahoma, USA, https://doi.org/10.2118/153869-MS.

Schechter, D., Zhou, D., Orr, F., 1994. Low ift drainage and imbibition. Journal

of Petroleum Science and Engineering 11 (4), 283 – 300, https://doi.org/10.1016/0920-4105(94)90047-7.

Shariatpanahi, S. F., Hopkins, P., Aksulu, H., Strand, S., Puntervold, T., Austad, T., 2016. Water based EOR by wettability alteration in dolomite. Energy & Fuels 30 (1), 180–187, https://doi.org/10.1021/acs.energyfuels.5b02239.

Shariatpanahi, S. F., Strand, S., Austad, T., 2011. Initial wetting properties of carbonate oil reservoirs: Effect of the temperature and presence of sulfate in formation water. Energy & Fuels 25 (7), 3021–3028, https://doi.org/10.1021/ef200033h.

Standnes, D., Austad, T., 2000. Wettability alteration in chalk. 1. preparation of core material and oil propeties. Journal of Petroleum Science and Engineering 28 (3), 111–121, https://doi.org/10.1016/S0920-4105(00)00083-8.

Strand, S., Austad, T., Puntervold, T., Høgnesen, E. J., Olsen, M., Barstad, Sven Michael, F., 2008. "Smart Water" for oil recovery from fractured limestone: A preliminary study. Energy & Fuels 22 (5), 3126–3133, https://doi.org/10.1021/ef800062n.

Strand, S., Standnes, D., Austad, T., 2006a. New wettability test for chalk based on chromatographic separation of SCN and $SO_4{}^{2-}$. Journal of Petroleum Science and Engineering 52 (1-4), 187–197, https://doi.org/10.1016/j.petrol.2006.03.021.

Strand, S., Standnes, D. C., Austad, T., 2003. Spontaneous imbibition of aqueous surfactant solutions into neutral to oil-wet carbonate cores: Effects of brine salinity and composition. Energy & Fuels 17 (5), 1133–1144, https://doi.org/10.1021/ef030051s.

Strand, S., Høgnesen, E. J., Austad, T., 2006b. Wettability alteration of carbonates - effects of potential determining ions (Ca^{2+} and $SO_4{}^{2-}$) and temperature. Colloids and Surfaces A: Physicochemical and Engineering Aspects 275 (1-3), 1 – 10, https://doi.org/10.1016/j.colsurfa.2005.10.061.

Fernø, M. A., Grnsdal, R., sheim, J., Nyheim, A., Berge, M., Graue, A., 2011. Use of sulfate for water based enhanced oil recovery during spontaneous imbibition in chalk. Energy & Fuels 25 (4), 1697–1706, https://doi.org/10.1021/ef200136w.

Høgnesen, E. J., Olsen, M., Austad, T., 2006. Capillary and gravity dominated flow regimes in displacement of oil from an oil-wet chalk using cationic surfactant. Energy & Fuels 20 (3), 1118–1122, https://doi.org/10.1021/ef050297s.

Torsæter, O., Abtahi, M., 2003. Experimental Reservoir Engineering Laboratory Work Book, 1st Edition. Norwegian University of Science and Technology, http://www.ipt.ntnu.no/~oletor/kompendium4015.pdf.

Thomas, M. M., Clouse, J. A., Longo, J. M., 1993. Adsorption of organic compounds on carbonate minerals: 1. model compounds and their influence on mineral wettability. Chemical Geology 109 (1-4), 201 – 213, https://doi.org/10.1016/0009-2541(93)90070-Y.

Weatherford International, 2013. Procedure for establishing initial water saturation when centrifuging. SCA-3009.

Yousef, A. A., Al-Saleh, S. H., Al-Kaabi, A., Al-Jawfi, M. S., 2011. Laboratory investigation of the impact of injection-water salinity and ionic content on oil recovery from carbonate reservoirs. SPE Reservoir Evaluation & Engineering 14 (05), 578–593, https://doi.org/10.2118/137634-PA.

Zeta Meter Inc, 2018. Zeta potential: A complete course in 5 minutes. The Double Layer, http://www.zeta-meter.com/5min.pdf.

Zhang, P., Austad, T., 2005. The relative effects of acid number and temperature on chalk wettability. SPE International Symposium on Oilfield Chemistry, 2-4 February, The Woodlands, Texas, https://doi.org/10.2118/92999-MS.

Zhang, P., Austad, T., 2006. Wettability and oil recovery from carbonates: Effects of temperature and potential determining ions. Colloids and Surfaces A: Physicochemical and Engineering Aspects 279 (1-3), 179 – 187, https://doi.org/10.1016/j.colsurfa.2006.01.009.

Zhang, P., Tweheyo, M. T., Austad, T., 2006. Wettability alteration and improved oil recovery in chalk: The effect of calcium in the presence of sulfate. Energy & Fuels 20 (5), 2056–2062, https://doi.org/10.1021/ef0600816.

Zhang, P., Tweheyo, M. T., Austad, T., 2007. Wettability alteration and improved oil recovery by spontaneous imbibition of seawater into chalk: Impact of the potential determining ions Ca^{2+}, Mg^{2+}, and ${SO_4}^{2-}$. Colloids and Surfaces A: Physicochemical and Engineering Aspects 301 (1-3), 199 – 208, https://doi.org/10.1016/j.colsurfa.2006.12.058.

Appendix A

Core Analysis Extra Data

Air permeability measurements

Figure 5.2 and Figure 5.3 were plotted based on the data presented in the tables below (from A.1 to A.8). This data is obtained during the air permeability measurements of the core plugs.

Table A.1: Results of air permeability measurements for core #B-1.

P_1 [bar]	P_2 [bar]	P_m [atm]	$1/P_m$ [atm]	Q [ml/s]	k_g [mD]
1.2	1.0	1.09	0.92	3.17	106.23
1.4	1.2	1.28	0.78	3.50	99.35
1.6	1.4	1.48	0.68	3.67	90.20
1.8	1.6	1.68	0.60	3.83	83.21

Table A.2: Results of air permeability measurements for core #B-2.

P_1 [bar]	P_2 [bar]	P_m [bar]	$1/P_m$ [atm]	Q [ml/s]	k_g [mD]
1.2	1.0	1.09	0.92	3.83	126.59
1.4	1.2	1.28	0.78	4.33	121.08
1.6	1.4	1.48	0.68	4.50	108.98
1.8	1.6	1.68	0.60	5.67	99.72

Table A.3: Results of air permeability measurements for core #B-3.

P_1 [bar]	P_2 [bar]	P_m [bar]	$1/P_m$ [atm]	Q [ml/s]	k_g [mD]
1.2	1.0	1.09	0.92	4.83	159.61
1.4	1.2	1.28	0.78	5.00	139.71
1.6	1.4	1.48	0.68	5.50	133.19
1.8	1.6	1.68	0.60	5.83	124.64

Table A.4: Results of air permeability measurements for core #B-4.

P_1 [bar]	P_2 [bar]	P_m [bar]	$1/P_m$ [atm]	Q [ml/s]	k_g [mD]
1.2	1.0	1.09	0.92	2.17	71.55
1.4	1.2	1.28	0.78	2.33	65.20
1.6	1.4	1.48	0.68	2.50	60.54
1.8	1.6	1.68	0.60	2.50	53.42

Table A.5: Results of air permeability measurements for core #B-5.

P_1 [bar]	P_2 [bar]	P_m [bar]	$1/P_m$ [atm]	Q [ml/s]	k_g [mD]
1.2	1.0	1.09	0.92	5.83	195.68
1.4	1.2	1.28	0.78	6.17	175.04
1.6	1.4	1.48	0.68	6.83	168.10
1.8	1.6	1.68	0.60	7.17	155.56

Table A.6: Results of air permeability measurements for core #B-6.

P_1 [bar]	P_2 [bar]	P_m [bar]	$1/P_m$ [atm]	Q [ml/s]	k_g [mD]
1.2	1.0	1.09	0.92	2.83	93.56
1.4	1.2	1.28	0.78	3.00	83.83
1.6	1.4	1.48	0.68	3.17	76.69
1.8	1.6	1.68	0.60	3.33	71.23

Table A.7: Results of air permeability measurements for core #B-7.

P_1 [bar]	P_2 [bar]	P_m [bar]	$1/P_m$ [atm]	Q [ml/s]	k_g [mD]
1.2	1.0	1.09	0.92	1.67	55.04
1.4	1.2	1.28	0.78	1.83	51.23
1.6	1.4	1.48	0.68	2.00	48.43
1.8	1.6	1.68	0.60	2.17	46.30

Table A.8: Results of air permeability measurements for core #B-8.

P_1 [bar]	P_2 [bar]	P_m [bar]	$1/P_m$ [atm]	Q [ml/s]	k_g [mD]
1.2	1.0	1.09	0.92	3.83	126.59
1.4	1.2	1.28	0.78	4.17	116.43
1.6	1.4	1.48	0.68	4.50	108.98
1.8	1.6	1.68	0.60	4.67	99.72

XRD Spectra

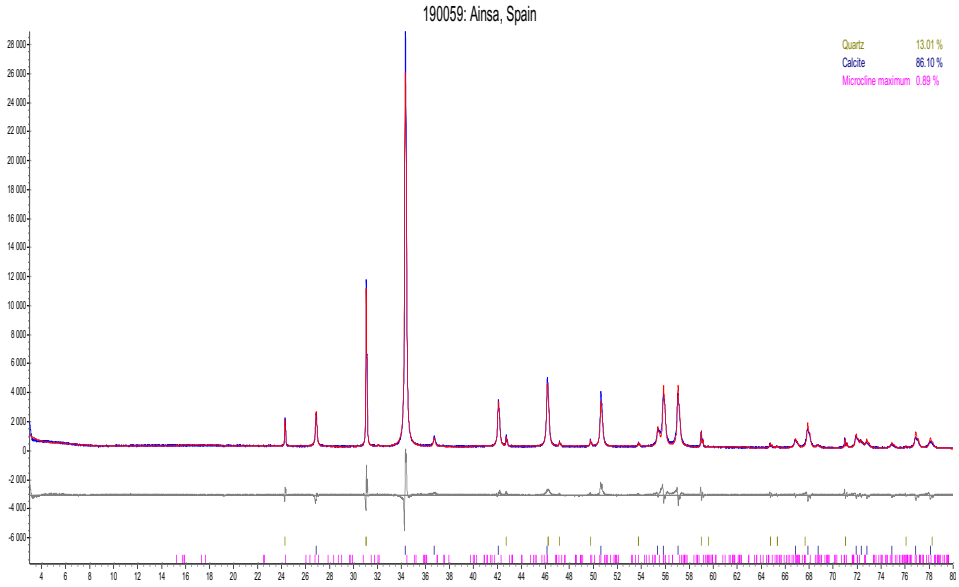

Figure A.1: XRD spectra of Ainsa carbonate rock powder.

Appendix B

Liquid Properties

Density

Density of liquids used in the experiments was measured using an Anton Paar density meter at 20 and 96°C. All liquids were degassed prior to measurements as described in subsection 4.2.1. The results are presented in Table B.1.

Table B.1: Results of density measurements.

Liquid	Oil	SFW	SSW	10dSSW	SSW2SO4	SSW4SO4
ρ at 20°C [g/cm^3]	0.92	1.17	1.02	1.00	1.02	1.02
ρ at 96°C [g/cm^3]	0.87	1.13	0.98	0.96	-	-

Viscosity

Dynamic viscosity, η, of the liquids used in the experiments was measured using rotational viscometer. The measurements were performed at a room temperature 21°C. However, temperature in the room varied $\pm$0.3°C from one test to another. The results are presented in Table B.2.

Table B.2: Results of dynamic viscosity measurements. Note that viscosity is presented in cP.

Liquid	Oil	SFW	SSW	10dSSW	SSW2SO4	SSW4SO4
η at 21°C [cP]	85	1.76	1.10	1.02	1.10	1.10

Appendix C

Young Equation

The Young equation expresses the contact angle in terms of the interfacial tensions between the solid and liquids. If the interfacial tensions are treated as forces and a horizontal force balance is applied (see Figure C.1), this yields to Equation C.1, reffered to as the Young equation.

$$\sigma_{os} = \sigma_{ws} + \sigma_{ow} \cos\theta \tag{C.1}$$

where

$$\begin{aligned} \cos\theta &= \text{cosine of the contact angle} && [-] \\ \sigma_{os} &= \text{oil/surface interfacial tension} && [mN/m] \\ \sigma_{ws} &= \text{water/surface interfacial tension} && [mN/m] \\ \sigma_{ow} &= \text{oil/water interfacial tension} && [mN/m] \end{aligned}$$

Rearranged Equation C.1 represents the contact angle:

$$\cos\theta = \frac{\sigma_{os} - \sigma_{ws}}{\sigma_{ow}} \tag{C.2}$$

The contact angle is measured through the denser fluid by convention, which is water in Figure C.1. The smaller the contact angle, the more water wet the rock surface.

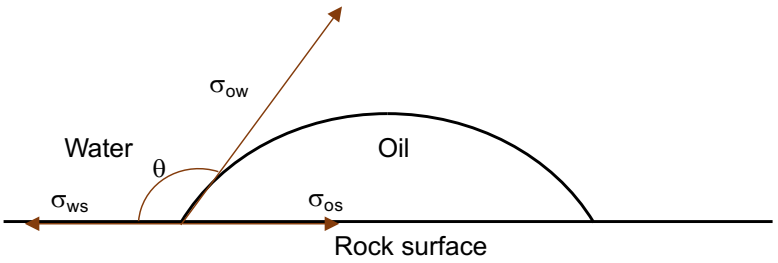

Figure C.1: Wettability of the oil-rock-brine system.